Ag^+ reduction and silver nanoparticle synthesis at the plasma-liquid interface by an RF driven atmospheric pressure plasma jet: mechanisms and the effect of surfactant

V. S. Santosh K. Kondeti,[1] Urvashi Gangal,[1] Shurik Yatom,[1] and Peter J. Bruggeman[1, a)]
Department of Mechanical Engineering, University of Minnesota, Minneapolis, USA.

(Dated: 27 June 2017)

The involvement of plasma produced species in the reduction of silver ions at the plasma-liquid interface is investigated using a well-characterized RF driven atmospheric pressure plasma jet. The absolute gas phase H density was measured using two photon absorption laser induced fluorescence in the free jet. Broadband absorption and transmission electron microscopy were used to study the synthesis of silver nanoparticles (AgNP). It is shown that fructose, an often used surfactant/stabilizer for AgNP synthesis, also acts as a reducing agent after plasma exposure. Nonetheless, surfactant free AgNP synthesis is observed. Several experimental findings indicate that H plays an important role in the reduction of silver ions for the plasma conditions in this study. VUV photons generated by the plasma are able to reduce silver ions in the presence of fructose. Adding H_2 to the argon feed gas leads to the production of a large amount of AgNPs having a particle size distribution with a maximum at a diameter of 2-3 nm, which is not observed for argon plasma. This finding is consistent with a smaller concentration of reducing species at the plasma-liquid interface for Ar with H_2 admixture plasma. The smaller flux of reactive species to the liquid is in this case due to a less strong interaction of the plasma with the liquid. The formation of the nanoparticles was observed even at a distance of 6-7 mm below the tip of the plasma plume, conditions not favoring the injection of electrons.

Keywords: Plasma, silver nanoparticles, electrons, atomic H, VUV, plasma liquid interaction

I. INTRODUCTION

Silver nanoparticles (AgNPs) possess unique optical, electrical and thermal properties having a wide range of applications ranging from photovoltaics, biological and chemical sensors to disinfection[1–3]. AgNPs are typically produced in Ag^+ containing solutions through the addition of a reducing agent to form silver atoms. The formed silver atoms coagulate and form AgNPs. Several chemical and physical methods have been used to reduce silver ions[4]. Nonetheless many AgNP syntheses processes use harmful reducing agents such as sodium borohydride and hydrazine and often produce hazardous by-products[5].

Plasmas can reduce silver ions and have the potential to generate AgNPs without any harmful byproducts. The synthesis of sub 10 nm AgNPs by plasma has previously been reported by Richmonds and Sankaran[6]. A surfactant/stabilizer such as fructose is often used in these studies to prevent uncontrolled particle growth and agglomeration[6–10]. Recent work suggests that gold nanoparticles may be electrostatically stabilized while AgNPs are stabilized by polymers or surfactants[11].

Solvated electrons generated by the plasma were suggested to be responsible for reducing silver ions[6]. Concentrations of solvated electrons of the order of 1 mM at the plasma-liquid interface have been reported for similar plasma conditions as used for AgNPs synthesis[12]. The solvated electrons, due to their short lifetime, are only present in a 10 nm layer at the plasma-liquid interface[12]. Apart from electrons, the plasma also transfers ions, long-lived reactive species, radicals and UV/VUV photons to the liquid. This results in a complex plasma-induced liquid chemistry[13]. The mixture of highly reactive species can reach large concentrations at the plasma-liquid interface. This results in competing radical reactions and large

a)Electronic mail: pbruggem@umn.edu.

concentration gradients rendering the identification of the species playing a role in the reduction of silver ions in solution complex.

One of the key species in plasma-liquid interaction is H [14]. The H radical is also the major reducing species in acidic solutions[15]. The hydrogen atom has a similar reduction potential as e^-_{aq} but its possible role in the reduction of Ag^+ has not been considered or analyzed.

Shirai *et al.*[16] have performed AgNP synthesis in a Hofmann electrolysis apparatus with two glow discharges acting as electrodes. They found that AgNPs were only produced at the anode and attribute the reduction of Ag^+ to electron injection. However, it has been reported that the flux of OH and H radicals is significantly larger for liquid cathode compared to liquid anode glow discharges[17,18]. These different neutral fluxes can shift balances between oxidizing and reducing capacity of the liquid interface. The analyses of the syntheses of AgNPs by, *in situ*, liquid cell TEM report both reduction by H and solvated electrons[19]. VUV photons also produce H and OH at the plasma-liquid interface. While OH radicals are not able to reduce Ag^+, they do react with hydrocarbon molecules such as the surfactant fructose (a ketonic monosaccharide) and can strongly impact H and e^-_{aq} concentrations at the plasma-liquid interface through radical-radical reactions.

In this paper, we present a study of the chemical mechanism of Ag^+ reduction and AgNPs formation by a well characterized RF atmospheric pressure plasma jet[20–28]. An additional advantage of the jet is that both remote and liquid touching conditions can be investigated allowing a straightforward assessment of the effect of VUV on AgNP synthesis. One of the goals of this work is to identify the major plasma species responsible for Ag^+ reduction and determine the role of the surfactant fructose in the process. Ar plasma and Ar + 0.64% H_2 plasma which produce significantly different gas phase H densities are compared. A second goal is to explore the possibility to synthesize AgNPs by plasma without the addition of a stabilizer/surfactant.

We first describe the study of AgNP synthesis in the presence of fructose, a representative condition for the majority of synthesis studies[6–10]. We show the strong involvement of fructose in the Ag^+ reduction process. Next we report the possibility to form AgNPs without surfactant/stabilizer and provide an assessment of the possible underlying processes. Before we embark on the analysis of the process of formation of AgNPs, we introduce the plasma jet setup and plasma conditions in addition to the various diagnostics and analysis procedures.

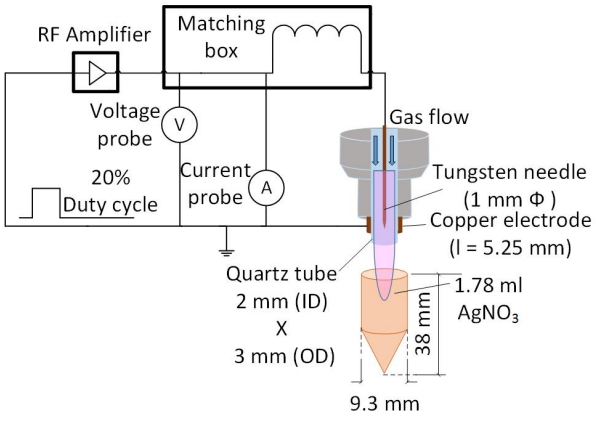

FIG. 1: Schematic of the RF plasma jet system and treatment conditions.

II. EXPERIMENTAL METHODS

A. PLASMA SOURCE

The atmospheric pressure plasma jet used in this work is shown in Figure 1. The plasma jet is identical to the setup used in[20]. It consists of a powered tungsten needle electrode ($\phi = 1$ mm) mounted inside a quartz tube with an inner diameter of 2 mm and an outer diameter of 3 mm. The gas flow is applied through the quartz tube. A copper ring electrode, connected to ground is mounted on the outside of the quartz tube. The total gas flow was maintained at 1.5 slm for all the conditions using a mass flow controller (MKS GE50A). In this work, we use Ar and Ar + 0.64% H_2 gas feeds. All measurements were performed in open air causing the presence of air impurities in the effluent. The relative humidity in the lab is 29%.

The plasma is generated by an RF (13.4 MHz) sinusoidal voltage wave modulated at a frequency of 20 kHz with a duty cycle of 20%. The plasma is thus off for 80% of the time. The RF voltage waveform is generated using a Tektronix AFC 3051 C function generator and is amplified by an RF amplifier (Amplifier Research 75A250A). A matching box consisting of an inductor is used to match the plasma jet with the power supply. Current and voltage waveforms were recorded with a Rogowski coil (Pearson 2877) and a voltage probe (Tektronix P5100A) to calculate the plasma dissipated power as described in[29]. The power shown in this work is the average power during the treatment time. Due to the presence of the grounded ring electrode, the plasma jet can be operated both remotely and in contact with the solution (touching). The plasma dissipated power when the jet is not touching the solution is 3.6 W throughout this work. The plasma dissipated power when touching the solution for the same settings of the power supply varies between 3.6 and 6.5W as a function of distance between the solution surface and the plasma jet nozzle. The detailed power values for all the measurement conditions are shown and discussed in the results section.

A 1 mM $AgNO_3$ + 10 mM fructose or a 20 mM $AgNO_3$ solution in distilled water with a volume of 1.78 ml was added to a centrifuge tube with a diameter (ϕ) of 9.3 mm and a depth of 38 mm and treated with the plasma jet. This volume filled the centrifuge tube completely. A schematic of the treatment conditions is shown in Figure 1. The distance between the nozzle and the liquid surface was varied between 4 and 22 mm. The treatment time was 10 and 5 minutes for solutions with and without fructose respectively. The maximum amount of solution evaporated during a treatment of 10 minutes is 0.35 ml, this corresponds to a distance of 5 mm between the nozzle and the liquid surface.

B. PLASMA CHARACTERIZATION

The head-on relative plasma emission intensity as seen by the solution was measured using an Avantes AvaSpec - 2048 spectrometer. A plastic tube with a length of 6 cm and a hole of 2 mm was placed in the effluent of the plasma plume to ensure that only emission from the jet in the axial direction was recorded. The optical fiber of the spectrometer along with a lens was attached to the other end of the tube. The measurements were performed by varying the distance between the entry hole of the tube and the plasma jet nozzle. The tube does not impact the plasma power.

The atomic H density was measured using two photon absorption laser induced fluorescence (TaLIF)[30]. For the detailed experimental procedure, the reader is referred to[31]. In short, a Nd:YAG laser operating at 532 nm (Spectra-Physics LAB-170-10H) pumps a dye laser (Sirah, Precision Scan) with a mixture of Rhodamine B and Rhodamine 101 dyes dissolved in ethanol resulting in fluorescence at 615 nm. This laser beam is subsequently doubled by a BBO crystal generating a second harmonic beam at 307.5 nm. The required 205 nm for TaLIF of H is subsequently produced by mixing the original 615 nm and 307.5 nm beam through another BBO crystal (Third Harmonic Generation). The ground state atomic H is excited to the 3d, 3p and 3s levels. When these excited states decay to 2s and 2p levels, fluorescence at 656.28 nm is observed. The absolute calibration is performed with krypton gas in a similar way as Niemi *et al.*[30]. The atomic H density (n_H) can be obtained by[30]:

$$n_H = \gamma \frac{\sigma^{(2)}_{Kr}}{\sigma^{(2)}_{H}} \frac{a_{Kr}}{a_H} \left(\frac{h\nu_H}{h\nu_{Kr}}\right)^2 \frac{S_H}{S_{Kr}} \frac{g(\Delta\nu)_{Kr}}{g(\Delta\nu)_H} n_{Kr} \quad (1)$$

where the subscripts H and Kr refer to atomic H and krypton respectively. γ is the transmission and collection efficiency of the detection, $\sigma^{(2)}$ is the photon excitation cross section, $h\nu$ is the photon energy, S is the fluorescence signal intensity and $g(\Delta\nu)$ is the overlap integral between the laser spectral profile and the two photon absorption profile as defined in[32]. The branching ratio (a) is defined as:

$$a_i = \frac{A_{ik}}{A_i + \sum_q k_q n_q} \quad (2)$$

where the subscript q refers to the quenching species, A_{ik} is the spontaneous emission coefficient of the observed fluorescence line (3s, 3p, 3d $\rightarrow$ 2s, 2p), A_i is the total spontaneous emission rate from the excited level (3d, 3p, 3s), k_q is the quenching coefficient and n_q is the density of the quenching species assuming that the 3-body collisional quenching is negligible[32].

The analysis considered the overlap integral and the quenching constants from literature for a known gas composition[24]. The air concentration in the jet effluent is taken from the reported measured air concentration of this jet[25]. Argon, oxygen, nitrogen and hydrogen were considered as the quenching species in the calculation of the collisional quenching rate. Considering that the cross section does not depend on the gas temperature, the quenching coefficient depends on the square root of the gas temperature[33]. The axial dependence of the gas temperature in the plasma jet was measured using Rayleigh scattering in a similar way as Verreycken *et al.*[34].

C. ANALYSIS OF NANOPARTICLES FORMATION

1. AgNPs DETECTION

The presence of AgNPs in solution produces a yellow colored solution due to surface plasmon resonance of the AgNPs. The absorbance has a maximum around a wavelength of 420 nm. A broadband light source (Energetiq LDLS) was focused on to a quartz cuvette (1 cm optical path-length) filled with plasma treated $AgNO_3$ solution to measure the absorbance with a spectrometer (Avantes AvaSpec - 2048). The absorbance depends on the size, concentration, size distribution, shape and possible agglomeration of the AgNPs[35–37]. The dielectric constant of the solution can also effect the plasmonic resonance[36]. An increased width of the absorption peak could be a result of a broader size distribution or a larger size of the AgNPs in the solution[38]. Absorbance measurements were performed to obtain a semi-qualitative estimation of the production of nanoparticles. While we present absorbance at 420 nm, the observed trends are identical for the wavelength integrated absorbance.

Transmission electron microscopy (TEM - FEI Tecnai T12) was performed for selected conditions to obtain the size distribution of the AgNPs. A few drops of the plasma treated solution were added on to a 300 mesh copper TEM grid (Electron Microscopy Sciences, Q325-CMA). The mesh was dried for an hour in the dark before TEM was performed. We collected at least ten TEM images of each sample to obtain a representative assessment of the size of the different particles in the sample. Particle size distribution of a few selected cases are also presented. These distributions were obtained by the image processing software ImageJ and Matlab. The particles were assumed to be spherical for the estimation of the diameter of the particles. The TEM images presented in the paper show an image that is representative of the majority of the observed particles. The high resolution images are included to show the plasma produced nanoparticles with the smallest observed size.

2. UV/VUV EMISSION

To investigate the effect of UV/VUV photons on the production of AgNPs, three different windows were individually placed on top of the liquid to pass photons with different wavelength ranges while blocking any flux of e^-, radicals and ions to the liquid surface. We used a Pyrex window transmitting photons with wavelengths $\geq$ 300 nm, a quartz window transmitting photons with wavelengths $\geq$ 200 nm and magnesium fluoride window transmitting photons with wavelengths $\geq$ 110 nm. We made sure that no gas bubble or layer was present between the window and the liquid to prevent the absorption of VUV photons before they reach the liquid surface. In addition, solution was added every 1.5 minutes to compensate for evaporation which prevented the formation of a gas or vapor bubble at the liquid-window interface.

3. SCAVENGER STUDY

Three different chemical scavengers were added to the $AgNO_3$ solution to investigate the role of the three key species potentially impacting directly or indirectly the reduction of silver ions: H, OH and e^-_{aq}. $NaNO_3$ scavenges H and e^-_{aq}. H_2O_2 scavenges H, OH and e^-_{aq} whereas 2-propanol effectively scavenges only H and OH and not e^-_{aq} [39]. The concentrations of the scavengers were varied between 0.25 mM to 100 mM to find effective scavenging conditions for each plasma condition. The reaction rate coefficients of the scavengers with H, OH and e^-_{aq} are shown and compared with the corresponding reaction rate coefficients of Ag^+ and D-fructose in Table I. The reaction rate coefficient of H with D-fructose is not reported and the reaction rate coefficient with glucose is provided as a reference.

TABLE I: Rate constants of the reactions of H, OH and e^-_{aq} with $NaNO_3$, H_2O_2, 2-propanol, D-fructose and Ag^+ [40].

	Species (Rate constant $M^{-1}s^{-1}$)		
Scavenger	H	OH	e^-_{aq}
$NaNO_3$	1.4×10^6	-	1.1×10^{10}
H_2O_2	9×10^7	2.7×10^7	1.2×10^{10}
2-Propanol	7.4×10^7	1.9×10^9	-
D-fructose	$^*6\times10^7$	1.6×10^9	$<1\times10^7$
Ag^+	2×10^{10}	1.2×10^{10}	4.2×10^{10}

*Estimation by analogy to glucose.

4. LIQUID ANALYSES

Aldehydes are known to be able to reduce Ag^+ [41]. Fructose could also be converted by the plasma to an aldehyde (R-CHO) group and become a reducing agent (see further). A colorimetric aldehyde assay kit, blue (Sigma Aldrich MAK140-1KT) was used to measure the concentration of aldehyde in the plasma treated solution containing fructose. The method of detection and calibration was performed as described in the Sigma Aldrich protocol[42]. A colorimetric solution (peak absorbance of 620 nm), that is proportional to the amount of aldehyde present in the solution is formed when an aldehyde reacts with this assay. The 620 nm photons were measured using a plate reader (Molecular Devices, Sunnyvale, CA, USA) in a 96 wells plate.

The pH of the plasma treated solution was measured using a pH probe (Thermo Scientific, Orion Star A215 with an Orion PerpHecT ROSS Combination pH Micro Electrode).

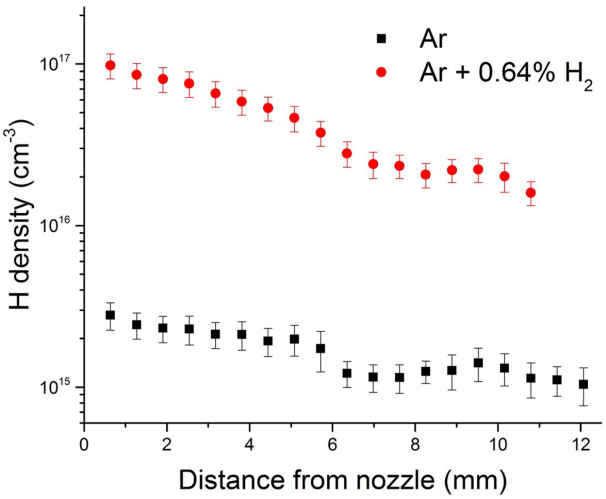

FIG. 2: Absolute atomic H density in the free jet effluent as a function of the distance from the jet nozzle for Ar and Ar + 0.64% H_2 plasma. The plasma power is 3.6 W.

III. RESULTS AND DISCUSSION

A. PLASMA CONDITIONS

In this work, we investigate both conditions for which the plasma is and is not in contact with the liquid/solution. These two conditions can produce significantly different species fluxes to the liquid. The difference between these two conditions is recognized by an increase in the plasma power when the plasma touches the liquid for fixed conditions of the power supply. The properties of the plasma in touching and non-touching mode are discussed separately in the following two sections.

1. NON-TOUCHING

The H density from the plasma was measured for Ar and Ar + 0.64% H_2 in the case of a free jet when no liquid was present close to the plasma plume. In the case of Ar, H is still produced due to the dissociation of trace impurities of water in the feed gas. The diffusion of humid air into the jet effluent can also lead to an enhancement of H formation in the jet effluent. The atomic H produced by Ar + 0.64% H_2 plasma is one order of magnitude higher than the case of Ar plasma (Figure 2). This suggests the possibility to assess the effect of H radicals on the reduction of Ag^+ by comparing Ar and Ar + 0.64% H_2 plasma treatments. The density of H produced by both Ar and Ar + 0.64% H_2 plasmas reduces with increasing distance from the jet nozzle similar to the trends observed for other species such as OH[43]. An increase in the plasma jet nozzle - liquid surface distance will reduce the flux of H, OH and e^- for non-touching conditions.

The H density is measured for a free jet without substrate while the treatments have a solution/substrate below the jet. The presence of solution/substrate changes the gas flow but does not significantly impact the density of the short lived species. This was verified for the OH radical[44]. In addition, the same approach has been used for the elucidation of the etching of polymers by O radicals with the same plasma jet[28]. This work yielded excellent agreement with the deduced O radical flux obtained from TaLIF measurements and the observed etching rate. Hence short-lived species measurements in the free jet can be used to obtain reliable estimates for non-touching plasma jets.

At a fixed plasma power, the electron density from the plasma will decrease with the increasing addition of molecular gases to Ar. This is due to the increased energy losses by vibrational excitation. The decrease in electron density is shown in[25] for a similar plasma jet operating in Ar with the addition of N_2, air and

O_2. The electron density in the plasma jet plume for the conditions studied in this work is approximately 10^{13} cm^{-3}, 2 to 4 orders of magnitude smaller than the H density shown in Figure 2[25]. The electron density quickly reduces in the effluent and transitions to an ion-ion plume (due to recombination and attachment to oxygen and/or water vapor)[45]. It was also shown that the ion concentration reduces by more than an order of magnitude over a distance of 3 mm from the visible plume tip[24] while the H density drops only by a factor of 0.3 over a distance of 3 mm from the tip of the visible plasma plume (Figure 2).

The Ar + 0.64% H_2 plasma produces UV continuum emission as shown in Figure 3. The intensity of UV emission reduces as the distance increases from the tip of the plasma jet nozzle. Although not shown in Figure 3, Ar plasma produces intense VUV excimer radiation at 124 nm[46]. The VUV emission will also reduce as a function of the distance from the nozzle due to an increased absorption of the VUV photons by an increasing air concentration as a function of distance from the nozzle[25].

2. TOUCHING

When plasma touches the liquid, the comparison between the Ar and Ar + 0.64 % H_2 jet becomes complex. It has been reported that when plasma is in contact with the solution, the flux of reactive species to the plasma-liquid interface can be orders of magnitude larger than for non-touching plasma conditions[45]. The production of H at the plasma-liquid interface due to ion recombination or photolysis[45] could dominate the H concentration in the liquid due to the flux of gas phase H radicals towards the liquid.

When the liquid is placed below the plasma, it results in an unknown water concentration in the region directly above the liquid surface. In this case, it is not possible to obtain the absolute H density at atmospheric pressure close to the interface with TaLIF due to an unknown effective lifetime of the excited state H atom, as H_2O is one of the main quenchers of H (n = 3)[47].

When the plasma touches the liquid, the discharge becomes more filamentary and the electron density will increase by an order of magnitude to a similar electron density as in a filamentary jet[25]. According to the simulations of Norberg *et al.*[45], the electron density at the liquid interface is at least 4 orders of magnitude smaller for non-touching compared to touching conditions while the radical flux to the liquid increases by ≈ 2 orders of magnitude.

The Ar excimer radiation can be a source of OH and H radicals in the solution particularly for small distances between the jet nozzle and the solution. The Ar excimer radiation at 124 nm can dissociate H_2O with a quantum yield of 0.93[14].

$$H_2O \xrightarrow{\text{VUV}} H + OH \tag{3}$$

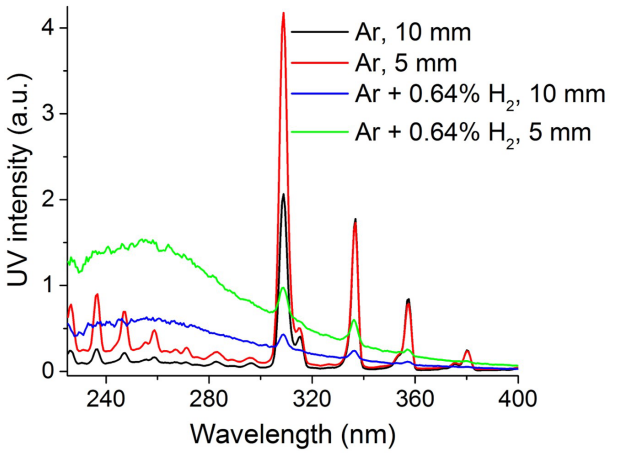

FIG. 3: Relative UV intensity for Ar and Ar + 0.64% H_2 plasma at 5 and 10 mm distance from the nozzle.

At small distances, the existence of an Ar channel between the nozzle and the liquid minimizes the absorption of the excimer emission by air.

B. NANOPARTICLE FORMATION IN THE PRESENCE OF FRUCTOSE

1. NANOPARTICLE PROPERTIES

A solution of 1 mM $AgNO_3$ + 10 mM fructose was treated with the plasma jet. The treatment time was 10 minutes per sample. The plasma treated solution has an absorbance with a maximum around a wavelength of 420 nm indicating the production of AgNPs (Figure 4). However the absorbance peak has a tail towards the higher wavelengths suggesting different AgNP sizes (see further).

When plasma touches the liquid, the liquid draws significantly higher current and the plasma power changes. The variation of the plasma power with distance between the solution and jet nozzle is shown in Figure 5. For closer distances, a significant increase in plasma power is observed in the case of Ar plasma. This is however not observed for the Ar + 0.64% H_2 plasma. The large variation in the plasma power observed at close distances between the plasma jet and the liquid is due to the movement of the liquid interface induced by the gas flow.

The liquid evaporates during the plasma treatment increasing the distance between the jet nozzle and liquid surface with treatment time. This leads to a distance range for which initially the plasma is touching the liquid while after some time, due to the evaporation of the liquid, the plasma is no longer in contact with the liquid surface (Figure 5).

The absorbance of the plasma treated solution at the end of the plasma treatment (Figure 5) reduces with increasing distance from the plasma jet nozzle. A significant change in absorbance is only found when the plasma is touching the liquid for distances smaller than the touching/non-touching transition region.

The absorbance as a function of distance in the case of Ar strongly correlates with the plasma dissipated power. Nonetheless a similar increase in absorbance at small distances is found for the Ar + 0.64% H_2 plasma without a significant increase in power. This suggests that both power and the increase in the interaction 'strength' of the plasma with the liquid contributes to the observed increase in absorbance of the treated solution. The variation in the power of Ar + 0.64% H_2 plasma is at most 12% whereas the variation in Ar is more significant but limited to a factor 1.5. Nonetheless, a stronger interaction with the liquid will lead

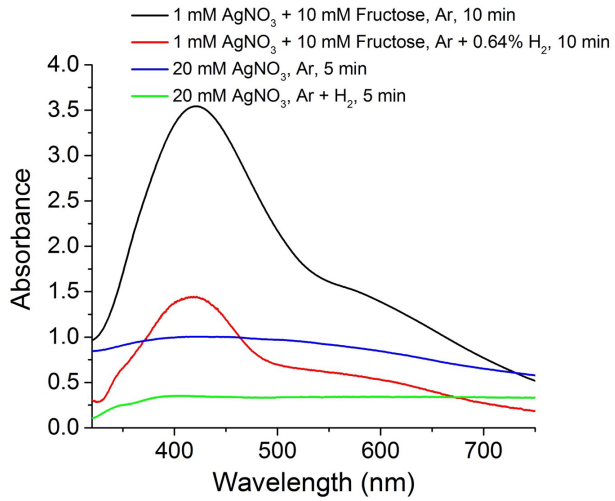

FIG. 4: Absorbance spectra of plasma treated $AgNO_3$ solutions for different plasma conditions in the presence and absence of fructose. The distance from the nozzle to the liquid surface is fixed at 5 mm and the plasma touches the liquid.

to a larger local power deposition at the plasma-liquid interface even at a constant total power.

As discussed in section III A, when the plasma is not in contact with the liquid, the flux of electrons impinging on to the liquid surface is also expected to be significantly smaller than the neutral flux of reactive species.

TEM images and particle size distribution confirm that both Ar and Ar + 0.64% H_2 plasmas for touching and non-touching conditions produce AgNPs (Figure 6). The tip of the plasma is at a distance of 6-7 mm from the solution in case of the non-touching conditions (Figure 6 (c), (d)). As apparent from the absorbance measurements, plasma touching the liquid increases the absorbance that is linked with an increase in the plasma power, radical and e^- flux. However nanoparticles are abundantly produced both with touching and non-touching plasma conditions in spite of the large change in electron flux between the touching and the non-touching conditions.

Figure 6 shows the particle size distribution corresponding to these TEM images for touching and non-touching conditions. Only particles with a diameter up to 40 nm have been considered as the amount of observed particles with a larger diameter is negligible. Significant differences in the particle size distribution are observed between touching and non-touching conditions and for Ar and Ar + 0.64% H_2 plasma. The Ar + 0.64% H_2 plasma in touching mode has a very pronounced particle distribution with a maximum at 2 nm while the Ar plasma in touching mode has a very broad distribution. Remarkably a particle size distribution dominated by smaller particles emerges for Ar plasma in non-touching mode while the narrow size distribution disappears for the Ar + 0.64% H_2 plasma in non-touching mode. We did not observe AgNPs with a diameter ≤ 5 nm in non-touching conditions.

AgNP growth during *in situ* liquid cell TEM at high beam current conditions ($3A/m^2$) followed a diffusion limited growth process[19]. Plasmas have typical current densities that surpass this value and the AgNP growth should thus be diffusion limited. The abundance of reducing agents produced by the plasma at the plasma-liquid interface rapidly reduces Ag^+ and the AgNP growth is limited by how fast the silver precursor can diffuse to the AgNP surface. In this case the growth rate will depend on the concentration of Ag and thus the concentrations of reducing agents will impact the final size of the AgNPs. As the convective and diffusive transport in the solution is similar for both treatments, the different minimum AgNP size for Ar and Ar + 0.64% H_2 relates to a different species flux (Figure 6 (a), (b)). The smaller size AgNPs in the case of Ar + 0.64% H_2 suggest a lower reactive species flux is impinging on the liquid for Ar + 0.64% H_2 as compared to Ar. This is consistent with the lower power of the plasma and its weaker contact with the solution which

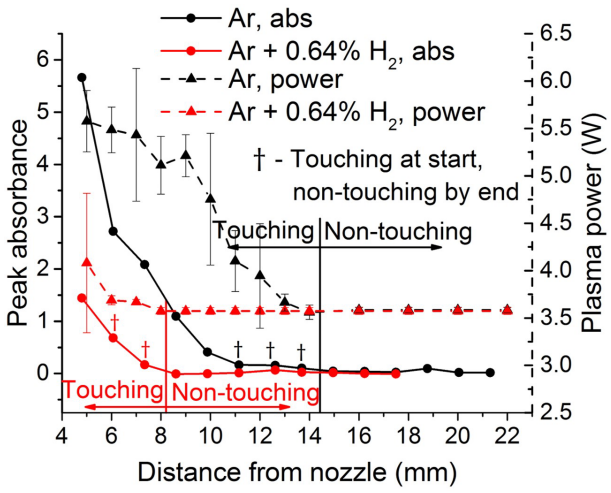

FIG. 5: Maximum absorbance at 420 nm of plasma treated 1 mM $AgNO_3$ + 10 mM fructose solution as a function of distance between the plasma jet nozzle and the solution. The results of Ar and Ar + 0.64% H_2 are depicted in black and red respectively. The corresponding plasma dissipated power for each condition is also provided. '†' denotes conditions for which the plasma was touching the liquid at the start of the treatment but was no longer in contact with the solution after a few minutes of treatment.

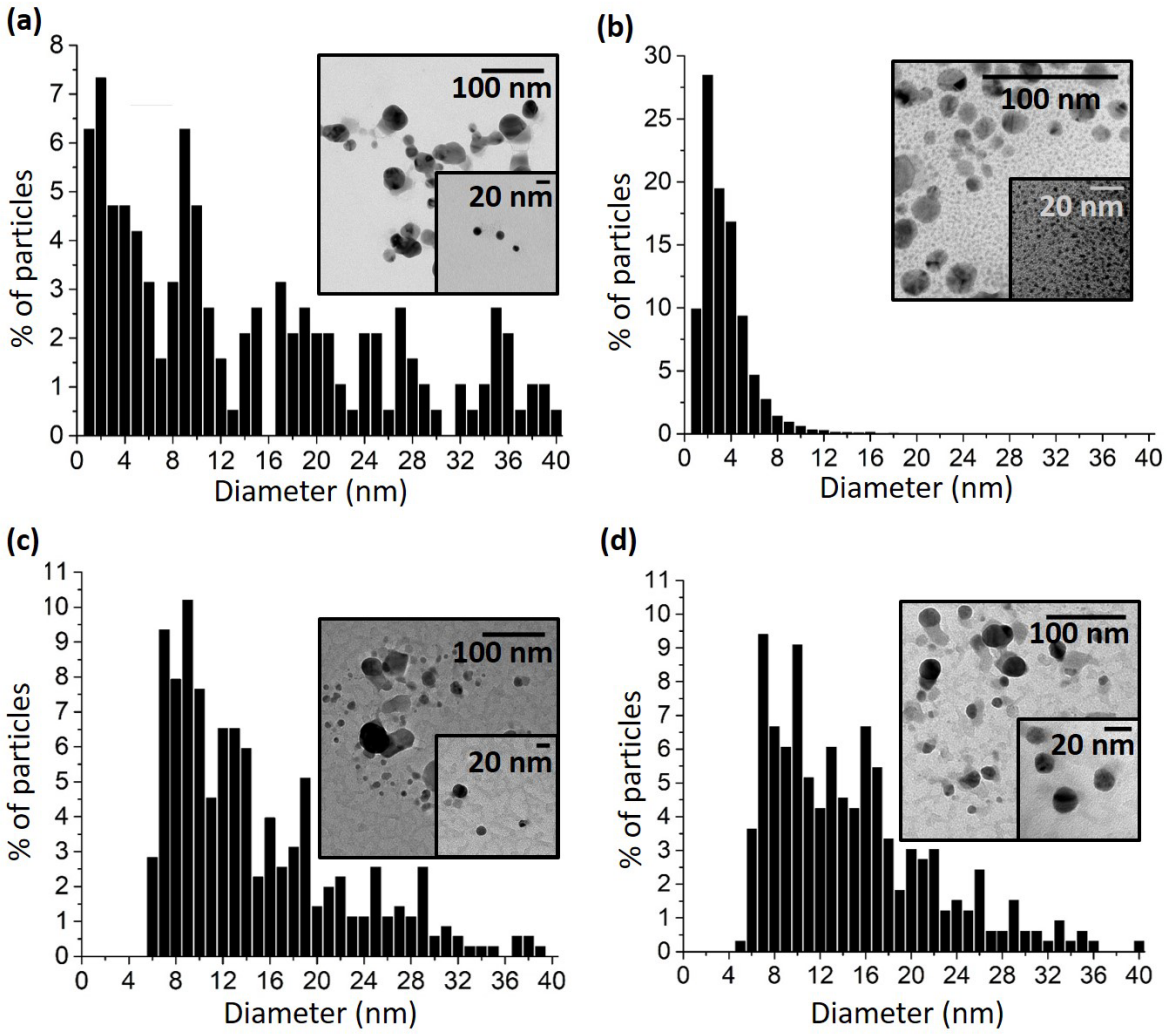

FIG. 6: TEM images and particle size distribution of AgNPs formed in 1 mM $AgNO_3$ + 10 mM fructose solution for a treatment time of 10 minutes. The feed gas and treatment distance are as follows: (a) Ar, 5 mm, (b) Ar + 0.64% H_2, 5 mm, (c) Ar, 20 mm, (d) Ar + 0.64% H_2, 15 mm.

is also illustrated by the absence of an increase in power for the Ar + 0.64% H_2 case. This conclusion is supported by the smaller particle size distribution observed for the Ar non-touching case compared to the touching case. Nonetheless, an opposite trend is observed in the case of Ar + 0.64% H_2. Fructose could also scavenge the plasma produced species reducing the concentration of the reducing agent.

2. MECHANISMS

In this section, we assess the effect of long-lived plasma produced species, VUV, fructose and the short-lived radicals H, OH and e^-_{aq} on the AgNP synthesis.

To assess the effect of long-lived plasma-produced reactive species, we treated distilled water with Ar and Ar + 0.64% H_2 plasma at 5 mm distance (touching). A solution of 100 μl of 1 mM $AgNO_3$ + 10 mM fructose was immediately added to the treated liquid. No change in the color of the solution is observed confirming

that the reduction process is dominantly initiated by short-lived reactive species. This role of short-lived species in the reduction of Ag^+ has also been found by de Vos *et al.*[11] unlike gold nanoparticles formation for which it was found that H_2O_2 is able to reduce Au^+ ions[48].

The effect of VUV is assessed by placing a magnesium fluoride window on top of the liquid. A brown layer of Ag or AgNPs was formed at the liquid-window interface (Figure 7 (a), (b)). Due to the lack of convection, as in the case of the direct treatment of the solution by plasma, the nanoparticles that are formed at the interface are not efficiently mixed in the solution and a brown layer is formed at the interface. When such treatment continued for over 30 minutes, the solution underneath the window started turning yellow. TEM images of such an indirect Ar plasma treated solution confirms AgNPs as in the case of a direct plasma treated solution (Figure 7 (c)). An absorbance measurement of such a solution also gave a similar absorbance curve profile as the direct plasma treated solutions (not shown). The change in the color of the solution was only observed for the Ar case. No production of AgNPs at the interface or a change of color or absorbance of the solution is observed with Pyrex and quartz windows even for prolonged treatment times in excess of 30 minutes. As discussed in section III A 2, VUV photons predominantly produce H and or OH at the liquid interface.

The H atoms can reduce silver ions:

$$Ag^+ + H \rightarrow Ag + H^+ \tag{4}$$

OH, being an oxidizer, cannot reduce silver ions although OH can react with fructose. When a magnesium fluoride window is placed on top of the solution, electron injection into the liquid does not occur, although solvated electrons can be generated with a quantum yield of 0.1 by photons of 124 nm from the Ar excimer radiation[14]. The production rate of solvated electrons by the Ar excimer radiation is thus nearly 10 times less than for H. In this case, considering the similar reaction rate coefficients (Table I) for the reduction of Ag^+ by H and e^-_{aq}, H dominates the reduction process over e^-_{aq}.

The absorbance of the AgNPs is much less with a magnesium fluoride window than for the case of direct plasma treatment in contact with the liquid. As the AgNPs size is similar (not shown), the reduced absorption suggests a reduced production rate of AgNPs. The reduced production rate of the AgNPs in the case of the magnesium fluoride window could be enhanced by the absorption of VUV photons in the AgNPs layer attached to the magnesium fluoride window after its formation. While we cannot make any quantitative statement on the relative importance of VUV compared to radicals, the results indicate that the VUV effect is stronger for Ar plasma compared to Ar + 0.64% H_2 plasma.

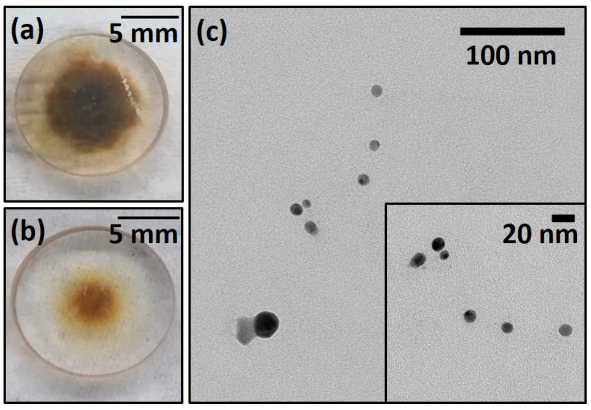

FIG. 7: (a), (b) Images of the magnesium fluoride window after treatment of 1 mM $AgNO_3$ + 10 mM fructose solution. The distance between the nozzle to the liquid surface covered with the magnesium fluoride window is 5 mm. The feed gas and treatment duration are as follows: (a) Ar, 5 minutes, (b) Ar + 0.64% H_2, 5 minutes. (c) TEM image of 30 minutes Ar plasma treatment of the solution covered by the magnesium fluoride window.

Fructose itself did not reduce Ag^+ for our conditions. However, plasma treated fructose added to a solution of $AgNO_3$ did lead to the reduction of Ag^+ and the formation of nanoparticles. A 100 μl solution of 0.1M $AgNO_3$ was added immediately after exposing 1.78 ml of 10 mM fructose solution respectively to Ar and Ar + 0.64% H_2 plasma for 10 minutes. The variation of absorbance at 420 nm for such a solution is shown in Figure 8. Note that a larger $AgNO_3$ concentration was necessary to visually observe the AgNP production in this case.

The plasma caused the formation of an aldehyde as is confirmed by a colorimetric aldehyde assay kit shown in Figure 8. Aldehydes are easily oxidized to acids and act as strong reducing agents. The presence of the hydrogen atom attached to the carbonyl group facilitates easy oxidation of aldehydes. The aldehyde (R−CHO) reduces Ag^+ as follows:

$$R - CHO + H_2O + 2Ag^+ \rightarrow R - CO_2H + 2H^+ + 2Ag \tag{5}$$

Ketones such as fructose do not have this hydrogen atom and are thus more resistant to oxidation and reduction of Ag^+ [49,50].

While fructose itself cannot reduce silver ions, fructose could be converted to glucose by tautoisomerism, a Tollen's type reaction where basic conditions help ketonic fructose to tautoisomerise to aldehydic glucose[51]. This typically requires an elevated liquid temperature (70° - 75° C) and basic pH[41,51,52], very different than the bulk properties of the plasma treated solution in this study.

One cannot rule out the possibility of having a local basic pH and localized heating of the solution at the plasma-liquid interface. Modelling efforts of Gopalakrishnan *et al.*[53] show that the pH can be orders of magnitude different between the interface and the bulk of the liquid when performing a H^+ scavenger study. For instance, with a bulk H^+ concentration of 20mM, the reaction rate of H^+ with e^-_{aq} and the production of OH^- is much faster than the transport of H^+ to the bulk of the liquid. This leads to a huge gradient of H^+ and pH between the near interface and the bulk of the liquid, the pH of the interface being much more basic.

Another pathway for the production of the aldehyde is through the radical reaction of the OH radical with fructose. The reaction is expected to be similar to the reaction of OH with simple alcohols and proceeds through hydrogen abstraction producing a radical[54]. These radicals could disproportionate, dimerize or through another radical termination reaction form an aldehyde[54]. An aldehyde can also be formed due to break up of the fructose chain during exposure to the plasma as observed by radiolysis studies of fructose[55].

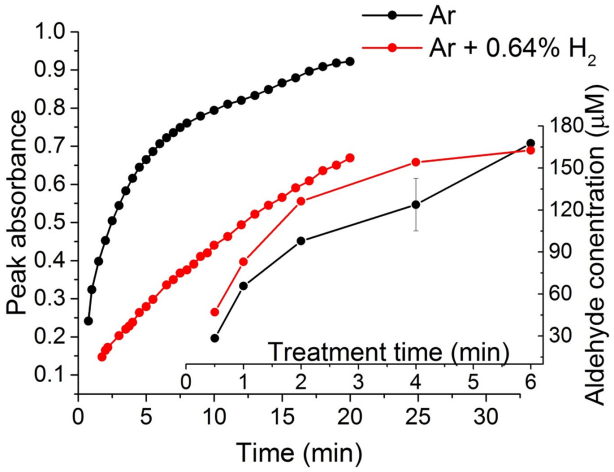

FIG. 8: Absorbance at 420 nm as a function of time elapsed after adding 100 μl of 0.1M $AgNO_3$ to a plasma treated solution containing 10 mM fructose (10 minutes treatment time). The inset shows the aldehyde concentration for different plasma treatment times. The treatment distance from the jet nozzle to the liquid is 5 mm.

The reaction rate coefficient of the solvated electrons with fructose is more than 4×10^{-3} times smaller than the reaction rate coefficient of the solvated electrons with Ag^+. The solvated electrons will react predominantly with Ag^+ instead of fructose in spite of its higher concentration for the direct plasma treatment. The reaction rate coefficient of H with fructose is not reported in literature, although it is likely similar to the reaction rate coefficient of H with glucose (6×10^7 $M^{-1}s^{-1}$)[40] making OH the most dominant reaction partner (reaction rate coefficient of 1.6×10^9 $M^{-1}s^{-1}$).

Apart from the reported stabilizing effect of fructose on the nanoparticles, fructose will predominantly react with OH radicals produced at the plasma-liquid interface and thus also act as a scavenger for OH radicals while producing an aldehyde that can enhance Ag^+ reduction.

To assess which other species are involved in the Ag^+ reduction (directly or through the formation of an aldehyde), three different chemical scavengers were added to the solution before treatment: $NaNO_3$, H_2O_2 and 2-propanol. All three scavengers gave a significant reduction in absorbance of the treated solution in spite of their difference in scavenging efficiencies for OH and e^-_{aq}. This suggests an important role of H in the reduction of Ag^+ (Figure 9) either directly by reaction 4 or through the formation of an aldehyde. A further and more detailed discussion of the involvement of these species in Ag^+ reduction will be provided in the next section that deals with AgNPs formation in the absence of fructose.

TEM images of the AgNPs produced by Ar + 0.64% H_2 plasma treated fructose (Figure 10 (b)) have a similar particle size distribution as the AgNPs produced by the direct plasma treatment of 1 mM $AgNO_3$ + 10 mM fructose (see Figure 6 (b)). While the particle size distribution is narrow, it does have an extended tail towards the higher particle size which is not present in the direct treatment of 1 mM $AgNO_3$ + 10 mM fructose by Ar + 0.64% H_2 plasma. This suggests that the particle size in the presence of fructose is not determined by the presence of short-lived species. In the case of the Ar plasma treatment of fructose only (Figure 10 (a)), the AgNPs have a narrow size distribution when compared to the AgNPs produced by the direct plasma treatment (Figure 6 (a)). This is in line with the formation of small nanoparticles for Ar with the reduction of the flux of reactive species. This difference, together with the requirement of a larger $AgNO_3$ concentration to achieve a visible change in the color of the solution indicates that in the direct plasma treatment, short-lived species contribute to the AgNPs production potentially including the formation of a hydrocarbon radical as an additional source of reduction.

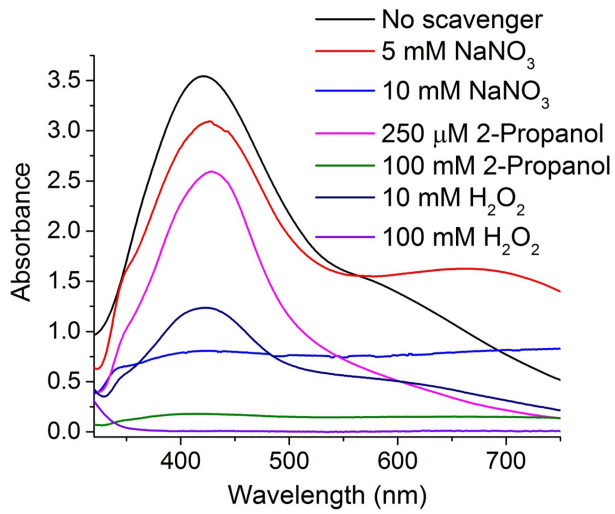

FIG. 9: Absorbance spectra of 1 mM $AgNO_3$ + 10 mM fructose containing $NaNO_3$, 2-propanol and H_2O_2 scavengers at the given concentrations after treatment by Ar plasma for 10 minutes. The treatment distance from the jet nozzle to the liquid is 5 mm.

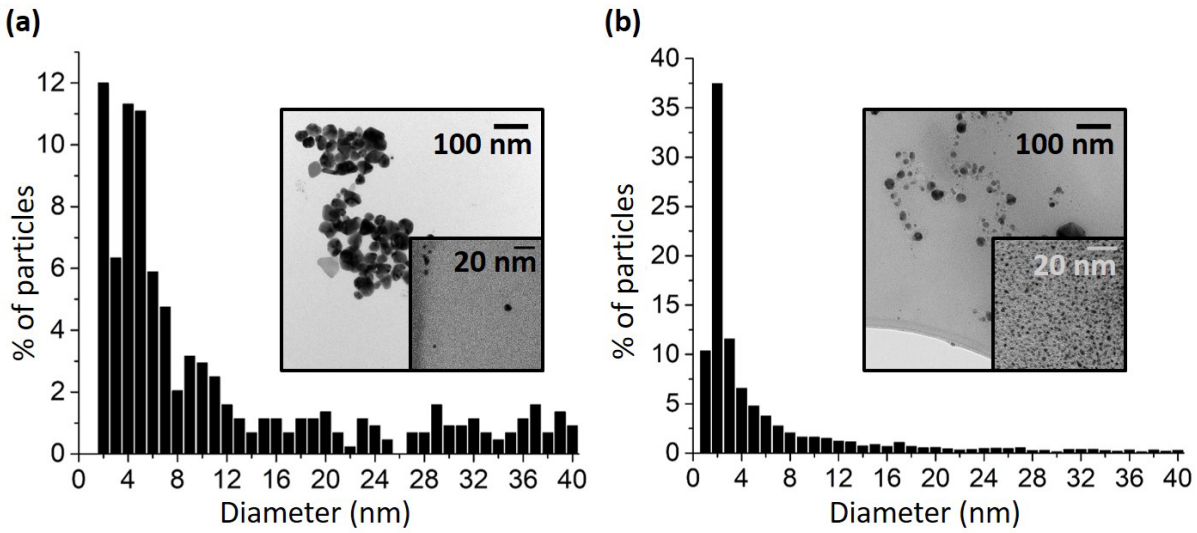

FIG. 10: TEM images and particle size distribution of AgNPs produced by plasma treated fructose after 30 minutes. For details, see text. The feed gas and treatment distance are as follows: (a) Ar, 5 mm, (b) Ar + 0.64% H_2, 5 mm.

C. NANOPARTICLE FORMATION IN THE ABSENCE OF FRUCTOSE

1. NANOPARTICLE PROPERTIES

As mentioned in the introduction, the majority of the reported AgNPs synthesis with plasma in aqueous solutions uses a stabilizer. However, the plasma jet used in this work is also able to produce AgNPs without a stabilizer/surfactant. While for solutions with fructose 1 mM $AgNO_3$ were used, the concentration of the solution had to be increased to 20 mM $AgNO_3$ in order to obtain an observable change in the color of the solution after plasma treatment in the absence of fructose. The treatment time was maintained at 5 minutes for these experiments. The required increase in Ag^+ supports the large involvement of fructose in the AgNP formation as shown before.

TEM images and particle size distributions of AgNPs produced in the absence of fructose are shown in Figure 11 for both touching and non-touching conditions. While larger particles and agglomeration of particles is observed than for solutions containing fructose, Ar + 0.64% H_2 plasma produces AgNPs with a particle size distribution having a maximum at 2-3 nm for both touching and non-touching conditions (Figure 11 (b), (d)). However comparing Figure 11 (b) with Figure 6 (b) shows that the presence of fructose suppresses the tail of the particle size distribution observed without fructose. This tail is also reduced when the species flux is smaller at larger distances (Figure 11 (d)). The Ar plasma produces a broader particle size distribution very similar to the case in the presence of fructose (Figure 11 (a), (c)).

2. MECHANISMS

Figure 12 shows the variation of the absorbance at 420 nm with increase in the concentration of 2-propanol, a scavenger of H and OH but not of e^-_{aq}. A higher concentration of 2-propanol is required for reducing the absorbance in the case of Ar + 0.64% H_2 plasma compared to the Ar plasma case. This is consistent with an expected higher H flux from Ar + 0.64% H_2 plasma or a more dominant effect of Ag^+ reduction by H compared to e^-_{aq} than in the case of Ar plasma. Adding the H_2O_2 scavenger yielded a similar reduction in absorbance as in the case with fructose in the solution although the reduction is already pronounced

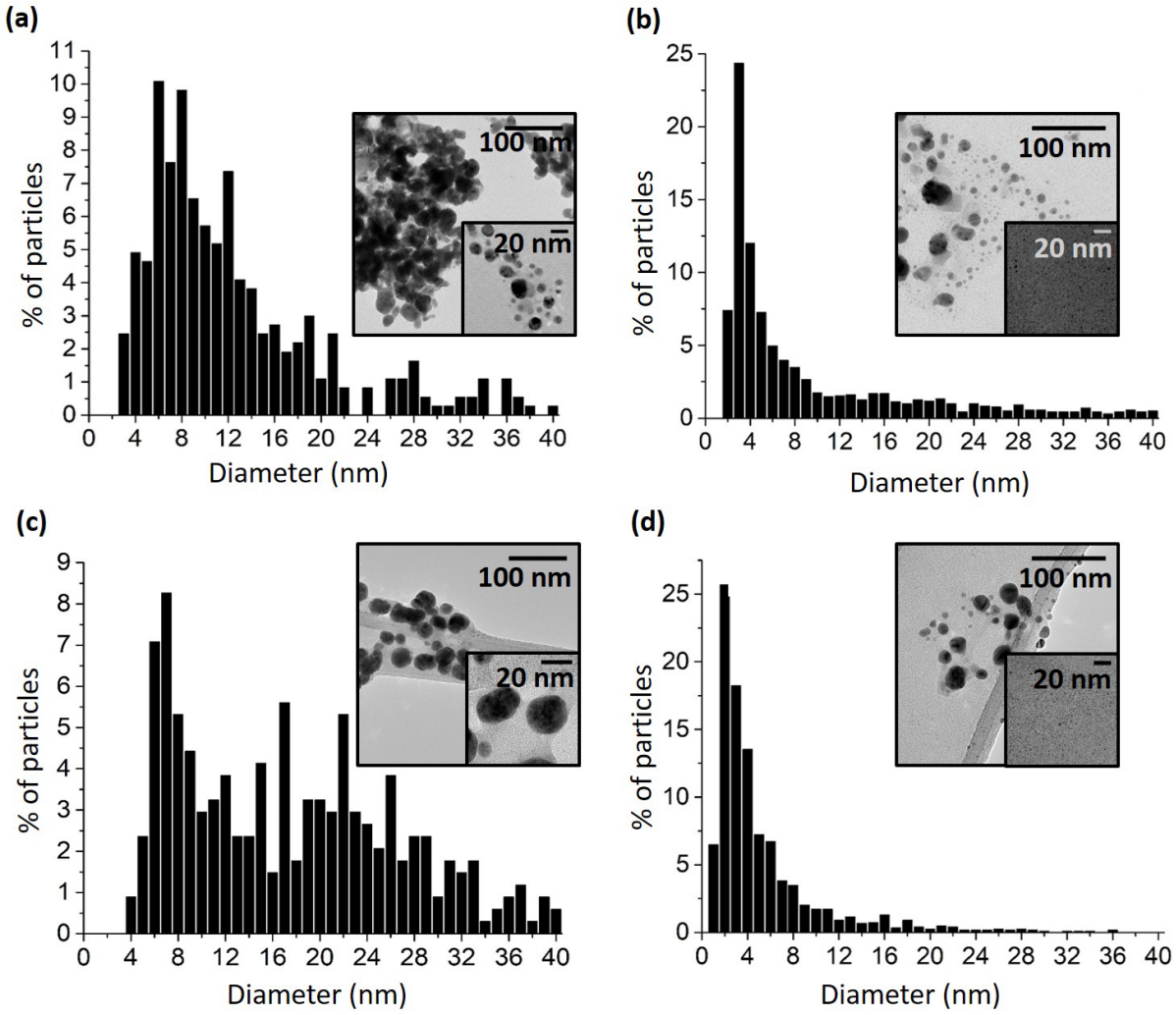

FIG. 11: TEM images and particle size distribution of AgNPs formed in 20 mM $AgNO_3$ solution for a treatment time of 5 minutes. The feed gas and treatment distance are as follows: (a) Ar, 5 mm, (b) Ar + 0.64% H_2, 4 mm, (c) Ar, 20 mm, (d) Ar + 0.64% H_2, 15 mm.

at approximately 10 times lower H_2O_2 concentrations (not shown). $NaNO_3$, however, gave a reduction in absorbance at low concentrations upto 10 mM $NaNO_3$, but the absorbance increased with a further increase in the concentration of $NaNO_3$. The exact reason for this particular observation is unclear.

The comparison of the H_2O_2 addition (that leads to e^-_{aq} scavenging) with the 2-propanol addition that yield similar effects on the absorbance suggest the importance of H radicals. While scavenger studies can often provide a good indication of the important reactive species in a process, the interpretation of the results remains challenging, particularly for short-lived species such as H, OH and e^-_{aq} that are present in high concentrations at the plasma-liquid interface. In this case, scavengers can be locally depleted or influence competing radical-radical reactions and 2-propanol could lead to radical formation that is involved in the reduction. This could for example be the cause of the non-monotonic behaviour of the absorbance observed in the case of Ar + 0.64% H_2 plasma with the addition of 2-propanol (Figure 12).

The pH of 20 mM $AgNO_3$ is 6.14 (Table II). The bulk concentration of Ag^+ is 3×10^4 times larger than that of H^+ suggesting that e^-_{aq} will react with Ag^+ rather than H^+. However, a depletion of Ag^+ ions

TABLE II: pH of the plasma treated 20 mM $AgNO_3$ solution. The distance between the nozzle and the solution is 5 mm for Ar and 4 mm for Ar + 0.64% H_2 for the touching conditions and 15 mm and 10 mm for non-touching conditions respectively. The treatment time is 5 minutes.

Condition	Initial pH	Final pH	
		Touching	Non-touching
Ar	6.14	7.39	6.64
Ar + 0.64% H_2		6.37	6.03

could occur at the interface due to rapid reduction by H and e^-_{aq} that is not compensated by the diffusion of bulk Ag^+ to the interface. This can result in significant gradients between the interface and the bulk of the solution. In the case that the Ag^+ concentration becomes smaller than the e^-_{aq} concentration at the interface, a dominant loss mechanism of solvated electrons in water leads to the production of OH^- [12]:

$$2e^-_{aq} + 2H_2O \rightarrow 2OH^- + H_2. \tag{6}$$

If H, OH and e^-_{aq} are present at similar concentrations, in view of the similar rate coefficients for these radicals in reactions with each other, radical-radical reactions such as

$$e^-_{aq} + H + H_2O \rightarrow OH^- + H_2 \tag{7}$$

and

$$e^-_{aq} + OH \rightarrow OH^- \tag{8}$$

occur and will also produce OH^-. This can lead to an increase in pH of the solution particularly for touching conditions coinciding with significant electron injection into the liquid. In the case of a dominance of H atoms, one anticipates that this increase in pH is partially compensated by the reduction of Ag^+ by H atoms leading to H^+ formation as in reaction 4. When solvated electrons are predominantly lost through

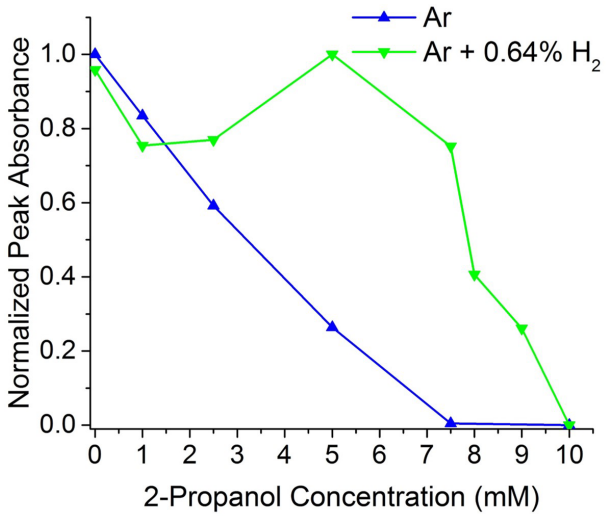

FIG. 12: Absorbance at 420 nm of the plasma treated solution containing 20 mM $AgNO_3$ as a function of the 2-propanol concentration. The treatment distance is 5 mm and 4 mm for the Ar and the Ar + 0.64% H_2 plasma treatment respectively.

the reaction with Ag^+, no change in pH is expected. The proposed reaction outcomes are consistent with the observed difference in the bulk pH of the solution after the Ar and the Ar+H_2 plasma treatment (Table II). The suggested depletion of the Ag^+ at the plasma-liquid interface is also in line with the observed pH values particularly for Ar plasma.

The increase in pH is only found for touching conditions for Ar + 0.64% H_2 plasma whereas the pH increases for both touching and non-touching conditions for Ar plasma. The Ar plasma will inject more electrons into the liquid in view of the stronger coupling with the liquid and the larger power than the Ar + 0.64% H_2 plasma. The magnitude of the increase in pH correlates with the higher e^- flux to the liquid.

As the treatments are performed in open air, acidification of the liquid could occur through the production of HNO_x and reduce the effect of pH increase due to e^- injection[56]. However the HNO_x production with Ar + 0.64% H_2 plasma should be similar to the Ar plasma[57] suggesting that the difference in pH between Ar and Ar + 0.64% H_2 plasma treated solutions relates to a difference in the flux of H and e^- to the liquid.

The treatment of the solution covered with a magnesium fluoride window did not yield any visible absorbance for a plasma power of 3.6 W unlike the case of fructose containing solutions. However, a brown layer, although much less pronounced as in the presence of fructose was formed for Ar at a plasma dissipated power of 5.5 W. VUV radiation likely does not play a dominant role in the reduction Ag^+ for the direct plasma treatment of $AgNO_3$ solution.

The concentration of solvated electrons for RF discharges is also anticipated to be smaller than for DC excited discharges that have been used for AgNP synthesis[6,16]. This is due to the alternating injection of electrons and ions in the liquid during one RF cycle causing an enhanced recombination of the solvated electrons at the interface with the impinging H_3O^+ ions from the plasma producing H radicals:

$$e^-_{aq} + H_3O^+ \rightarrow H + H_2O \tag{9}$$

The importance of H for Ag^+ reduction as suggested by the scavenger results in the present study that has not been found in previous studies such as[16,17] depends on the plasma properties and might be enhanced by the RF excitation and the 2 to 4 orders of magnitude higher gas phase H density than e^- density. Particularly the study of Mededovic *et al.* shows a strong effect of pH and polarity in favor of a e^-_{aq} induced reduction of Ag^+ for pulsed discharges in liquids. However, the electron density in such discharges is large with reported values in excess of 10^{19} cm^{-3} and similar densities for H deduced from models which would indeed be more favorable for an e^- induced reduction of Ag^+ [58,59].

IV. CONCLUSIONS

In this manuscript, we have shown that fructose can act as a surfactant, a scavenger for OH and a reducing agent through the formation of an aldehyde during plasma exposure by the plasma produced OH (and H) radicals. The RF atmospheric pressure plasma jet used in this work is also able to produce surfactant free AgNPs.

The differences in the particle size distribution of AgNPs produced by Ar and Ar + 0.64% H_2 plasma correlate with a different density of reducing agents produced by the plasma. A significant amount of small AgNPs having a narrow particle size distribution with a maximum at a diameter of 2-3 nm were synthesized using Ar + 0.64% H_2 plasma while for Ar plasma the observed particle size distribution is very broad. This result is consistent with the strong interaction of the Ar plasma with the solution at close distances between the plasma jet nozzle and the liquid leading to an enhanced production of the reducing species compared to the Ar + 0.64% H_2 plasma. A similar particle size distribution is found for Ar + 0.64% H_2 plasma both for touching and non-touching conditions. For the non-touching condition, the tip of the plasma plume is 7 mm away from the solution, a condition not favoring injection of electrons into the liquid.

While we cannot exclude the importance of solvated electrons in the reduction of Ag^+, several reported experimental findings suggest the importance of H in the reduction process particularly for an Ar + 0.64% H_2 plasma. These findings include the less pronounced coupling of the discharge with the solution combined with the higher gas phase H density, the lack of increase in pH as found for Ar plasma and the suppression of the AgNP formation by 2-propanol, a scavenger of H and OH but not for solvated electrons. The larger

relative importance of H compared to previous work is suggested to be due to the use of RF excitation and a gas phase H/e^- density ratio that amounts to 10^4.

A further analysis of the Ag^+ reduction process requires detailed kinetic modeling of the liquid phase kinetics which is planned for the future.

V. ACKNOWLEDGEMENTS

This work is partially funded by the University of Minnesota and the Department of Energy Plasma Science Center through the US Department of Energy, Office of Fusion Energy Sciences, Contract: DE-SC0001939. The TEM measurements have been performed at the Characterization Facility, University of Minnesota, which receives partial support from NSF through the MRSEC program. One of the authors (U.G.) gratefully acknowledges the technical advise of Professor Susanta K. Sen Gupta from Banaras Hindu University, India for discussions on the plasma induced liquid phase chemistry relevant to Ag^+ reduction.

[1] D. D. Evanoff and G. Chumanov, ChemPhysChem **6**, 1221–1231 (2005).
[2] B. V. K. Naidu, J. S. Park, S. C. Kim, S.-M. Park, E.-J. Lee, K.-J. Yoon, S. J. Lee, J. W. Lee, Y.-S. Gal, and S.-H. Jin, Solar Energy Mat. and Solar Cells **92**, 397–401 (2008).
[3] S. Prabhu and E. K. Poulose, Intl. Nano Lett. **2**, 1–10 (2012).
[4] S. Iravani, H. Korbekandi, S. Mirmohammadi, and B. Zolfaghari, Research in Pharma. Sci. **9**, 385 (2014).
[5] P. Rauwel, S. Küünal, S. Ferdov, and E. Rauwel, Adv. in Mat. Sci. and Eng. **2015** (2015).
[6] C. Richmonds and R. M. Sankaran, Appl. Phys. Lett. **93**, 131501 (2008).
[7] W.-H. Chiang, C. Richmonds, and R. M. Sankaran, Plasma Sources Sci. Technol. **19**, 034011 (2010).
[8] X. Z. Huang, X. Zhong, Y. Lu, Y. S. Li, A. E. Rider, S. A. Furman, and K. Ostrikov, Nanotechnology **24**, 095604 (2013).
[9] F.-C. Chang, C. Richmonds, and R. M. Sankaran, J. Vac. Sci. & Technol. A: Vac., Surf., and Films **28**, L5–L8 (2010).
[10] Q. Chen, J. Li, and Y. Li, J. Phys. D: Appl. Phys. **48**, 424005 (2015).
[11] C. De Vos, J. Baneton, M. Witzke, J. Dille, S. Godet, M. J. Gordon, R. M. Sankaran, and F. Reniers, J. Phys. D: Appl. Phys. **50**, 105206 (2017).
[12] P. Rumbach, D. M. Bartels, R. M. Sankaran, and D. B. Go, Nature Communications **6** (2015).
[13] S. Samukawa, M. Hori, S. Rauf, K. Tachibana, P. Bruggeman, G. Kroesen, J. C. Whitehead, A. B. Murphy, A. F. Gutsol, S. Starikovskaia, *et al.*, J. Phys. D: Appl. Phys. **45**, 253001 (2012).
[14] P. J. Bruggeman, M. J. Kushner, B. R. Locke, J. Gardeniers, W. Graham, D. B. Graves, R. C. Hofman-Caris, D. Maric, J. P. Reid, E. Ceriani, *et al.*, Plasma Sources Sci. Technol. **25**, 053002 (2016).
[15] G. V. Buxton, C. L. Greenstock, W. P. Helman, and A. B. Ross, J. Phys. and Chem. Ref. Data **17**, 513–886 (1988).
[16] N. Shirai, S. Uchida, and F. Tochikubo, Jap. J. Appl. Phys. **53**, 046202 (2014).
[17] S. M. Thagard, K. Takashima, and A. Mizuno, Plasma Chem. and Plasma Process. **29**, 455–473 (2009).
[18] O. Polyakov, A. Badalyan, and L. Bakhturova, High Energy Chem. **37**, 322–327 (2003).
[19] T. J. Woehl, J. E. Evans, I. Arslan, W. D. Ristenpart, and N. D. Browning, ACS nano **6**, 8599–8610 (2012).
[20] C. Van Gils, S. Hofmann, B. Boekema, R. Brandenburg, and P. Bruggeman, J. Phys. D: Appl. Phys. **46**, 175203 (2013).
[21] S. Zhang, A. Sobota, E. van Veldhuizen, and P. Bruggeman, Plasma Sources Sci. Technol. **24**, 045015 (2015).
[22] S. Zhang, W. van Gaens, B. van Gessel, S. Hofmann, E. van Veldhuizen, A. Bogaerts, and P. Bruggeman, J. Phys. D: Appl. Phys. **46**, 205202 (2013).
[23] A. Van Gessel, K. Alards, and P. Bruggeman, J. Phys. D: Appl. Phys. **46**, 265202 (2013).
[24] B. Van Ham, S. Hofmann, R. Brandenburg, and P. Bruggeman, J. Phys. D: Appl. Phys. **47**, 224013 (2014).
[25] B. van Gessel, R. Brandenburg, and P. Bruggeman, Appl. Phys. Lett. **103**, 064103 (2013).
[26] J. J. Wu, V. S. S. K. Kondeti, P. J. Bruggeman, and U. R. Kortshagen, J. Phys. D: Appl. Phys. **49**, 08LT02 (2016).
[27] A. J. Knoll, P. Luan, E. A. Bartis, V. S. Kondeti, P. J. Bruggeman, and G. S. Oehrlein, Plasma Proc. and Poly. (2016).
[28] P. Luan, A. Knoll, H. Wang, V. Kondeti, P. Bruggeman, and G. Oehrlein, J. Phys. D: Appl. Phys. **50**, 03LT02 (2016).
[29] S. Hofmann, A. Van Gessel, T. Verreycken, and P. Bruggeman, Plasma Sources Sci. Technol. **20**, 065010 (2011).
[30] K. Niemi, V. Schulz-Von Der Gathen, and H. Döbele, J. Phys. D: Appl. Phys. **34**, 2330 (2001).
[31] S. Yatom, Y. Luo, Q. Xiong, and P. Bruggeman, "(in preparation)," (2017).
[32] J. B. Schmidt, *Ultrashort Two-Photon-Absorption Laser-Induced Fluorescence in Nanosecond-Duration, Repetitively Pulsed Discharges*, Ph.D. thesis, The Ohio State University (2015).
[33] H. Döbele, T. Mosbach, K. Niemi, and V. Schulz-Von Der Gathen, Plasma Sources Sci. Technol. **14**, S31 (2005).
[34] T. Verreycken, A. Van Gessel, A. Pageau, and P. Bruggeman, Plasma Sources Sci. Technol. **20**, 024002 (2011).
[35] W. Haiss, N. T. Thanh, J. Aveyard, and D. G. Fernig, Anal. Chem. **79**, 4215–4221 (2007).
[36] K. L. Kelly, E. Coronado, L. L. Zhao, G. C. Schatz, *et al.*, J. Phys. Chem. B-Condensed Phase **107**, 668–677 (2003).
[37] T. Jensen, L. Kelly, A. Lazarides, and G. C. Schatz, J. Cluster Sci. **10**, 295–317 (1999).
[38] N. S. Pesika, K. J. Stebe, and P. C. Searson, J. Phy. Chem. B **107**, 10412–10415 (2003).
[39] J. W. T. Spinks and R. J. Woods, *An introduction to radiation chemistry* (John Wiley & Sons, 1990).
[40] "http://kinetics.nist.gov/solution/," NDRL/NIST Solution Kinetics Database.

[41]S. Panigrahi, S. Kundu, S. K. Ghosh, S. Nath, and T. Pal, Colloids and Surf. A: Physico. and Eng. Asp. **264**, 133–138 (2005).
[42]"www.sigmaaldrich.com/catalog/product/sigma/mak140," Sigma Aldrich, MAK140-1KT.
[43]T. Verreycken, R. Mensink, R. Van Der Horst, N. Sadeghi, and P. J. Bruggeman, Plasma Sources Sci. Technol. **22**, 055014 (2013).
[44]V. Kondeti and P. J. Bruggeman, Unpublished results.
[45]S. A. Norberg, W. Tian, E. Johnsen, and M. J. Kushner, J. Phys. D: Appl. Phys. **47**, 475203 (2014).
[46]A. El-Habachi and K. H. Schoenbach, Appl. Phys. Lett. **72**, 22–24 (1998).
[47]J. Bittner, K. Kohse-Höinghaus, U. Meier, and T. Just, Chem. Phys. Letters **143**, 571–576 (1988).
[48]J. Patel, L. Němcová, P. Maguire, W. Graham, and D. Mariotti, Nanotechnology **24**, 245604 (2013).
[49]E. Filippo, A. Serra, A. Buccolieri, and D. Manno, J. Non-Crystalline Solids **356**, 344–350 (2010).
[50]Z.-m. Qi, H.-s. Zhou, N. Matsuda, I. Honma, K. Shimada, A. Takatsu, and K. Kato, J. Phys. Chem. B **108**, 7006–7011 (2004).
[51]V. K. Sharma, R. A. Yngard, and Y. Lin, Adv. Colloid and Interf. Sci. **145**, 83–96 (2009).
[52]S. Panigrahi, S. Kundu, S. Ghosh, S. Nath, and T. Pal, J. Nano. Research **6**, 411–414 (2004).
[53]R. Gopalakrishnan, E. Kawamura, A. Lichtenberg, M. Lieberman, and D. Graves, J. Phys. D: Appl. Phys. **49**, 295205 (2016).
[54]V. I. Parvulescu, M. Magureanu, and P. Lukes, *Plasma chemistry and catalysis in gases and liquids* (John Wiley & Sons, 2012).
[55]G. Phillips and G. Moody, J. Chem. Society , 754–761 (1960).
[56]P. Rumbach, M. Witzke, R. Sankaran, and D. Go, J. American Chem. Soc. **135**, 16264–16247 (2013).
[57]K. Wende, P. Williams, J. Dalluge, W. Van Gaens, H. Aboubakr, J. Bischof, T. von Woedtke, S. M. Goyal, K.-D. Weltmann, A. Bogaerts, *et al.*, Biointerphases **10**, 029518 (2015).
[58]S. Medodovic and B. Locke, J. Phys. D: Appl. Phys. **42**, 049801 (2009).
[59]P. Bruggeman and C. Leys, J. Phys. D: Appl. Phys. **42**, 053001 (2009).

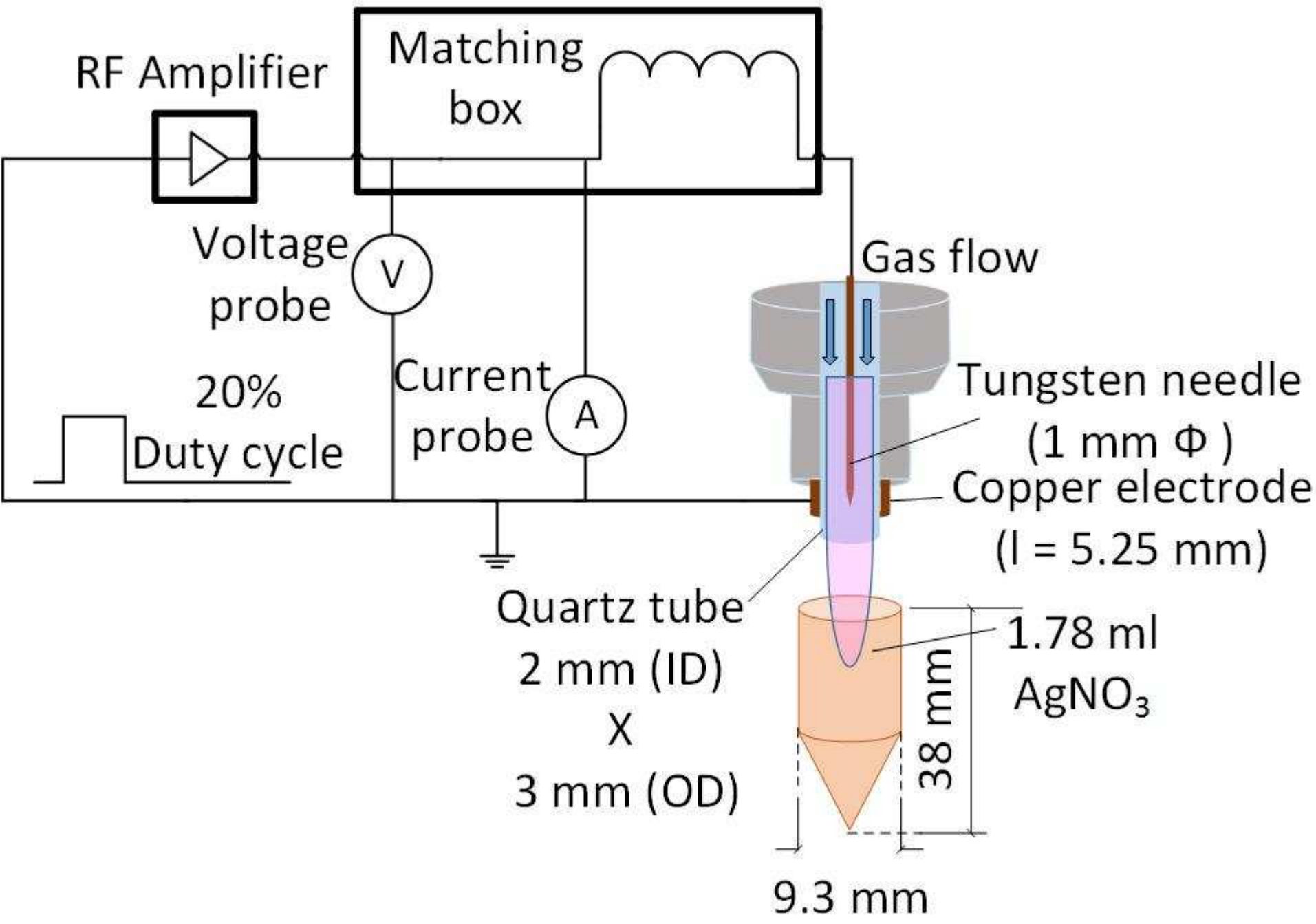
RF Amplifier
Matching box
Voltage probe
V
Current probe
A
20%
Duty cycle
Gas flow
Tungsten needle
(1 mm Φ)
Copper electrode
(l = 5.25 mm)
Quartz tube
2 mm (ID)
X
3 mm (OD)
1.78 ml
AgNO3
38 mm
9.3 mm

Ar

Ar + 0.64% H_2

H density (cm^{-3})

10^{17}

10^{16}

10^{15}

0

2

4

6

8

10

12

Distance from nozzle (mm)

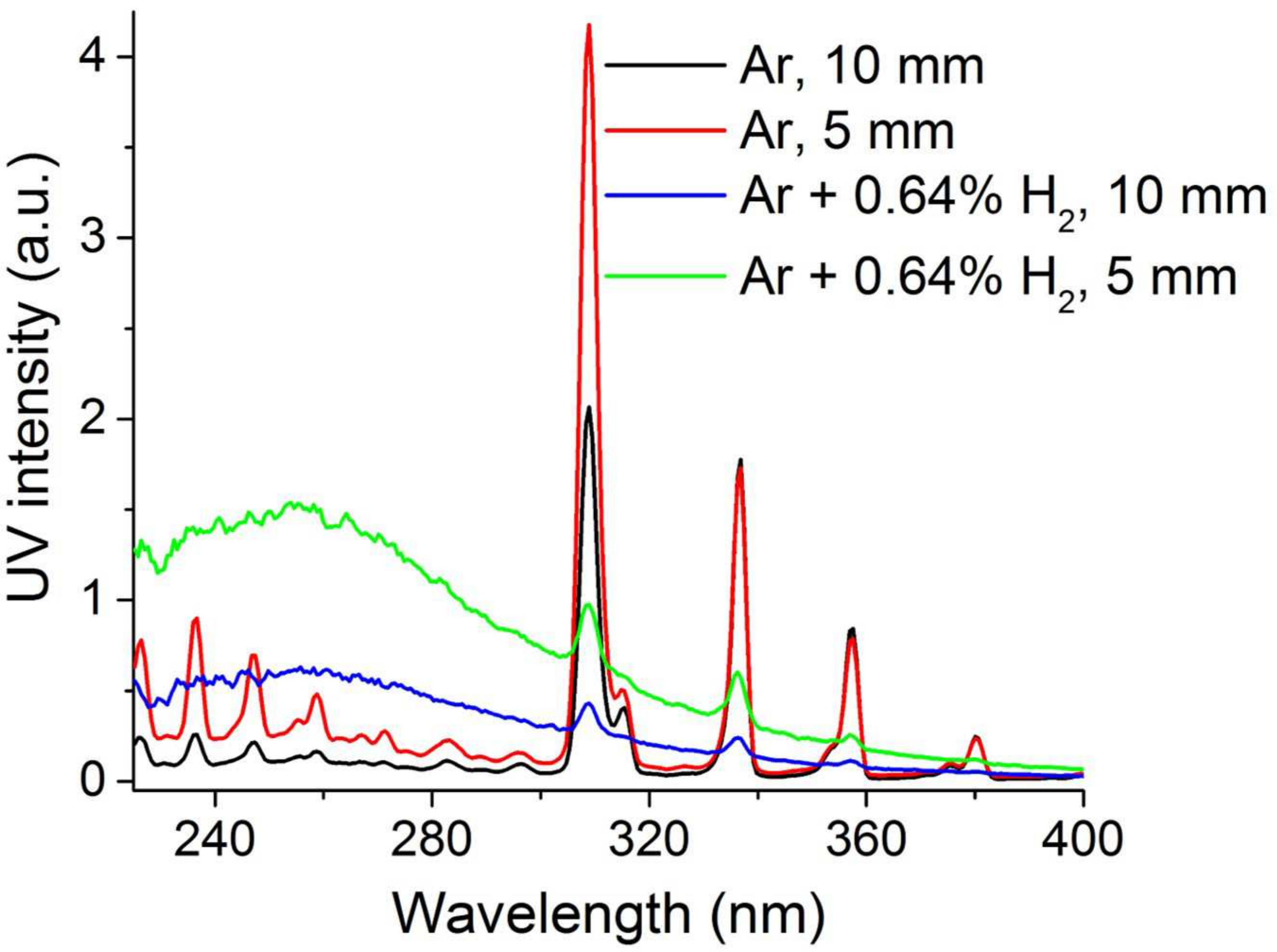
Ar, 10 mm
Ar, 5 mm
Ar + 0.64% H2, 10 mm
Ar + 0.64% H2, 5 mm
UV intensity (a.u.)
0
1
2
3
4
240
280
320
360
400
Wavelength (nm)

1 mM $AgNO_3$ + 10 mM Fructose, Ar, 10 min
1 mM $AgNO_3$ + 10 mM Fructose, Ar + 0.64% H_2, 10 min
20 mM $AgNO_3$, Ar, 5 min
20 mM $AgNO_3$, Ar + H_2, 5 min

Absorbance

4.0
3.5
3.0
2.5
2.0
1.5
1.0
0.5
0.0

400
500
600
700

Wavelength (nm)

Ar, abs
Ar + 0.64% H_2, abs
Ar, power
Ar + 0.64% H_2, power
† - Touching at start, non-touching by end
Touching | Non-touching
Touching Non-touching
Peak absorbance
Plasma power (W)
Distance from nozzle (mm)
0
1
2
3
4
5
6
2.5
3.0
3.5
4.0
4.5
5.0
5.5
6.0
6.5
4
6
8
10
12
14
16
18
20
22

(a)

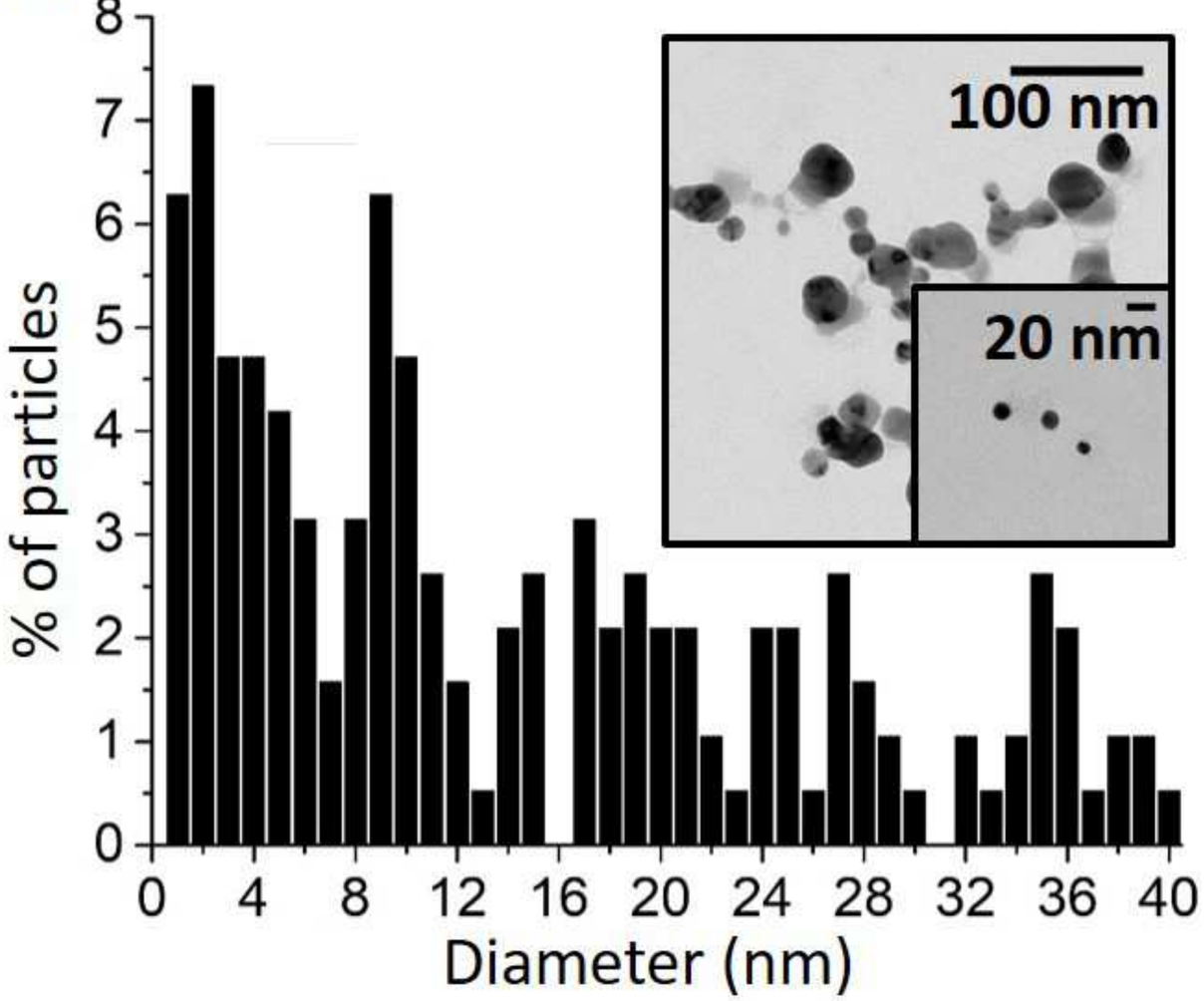
% of particles
Diameter (nm)
100 nm
20 nm

(b)

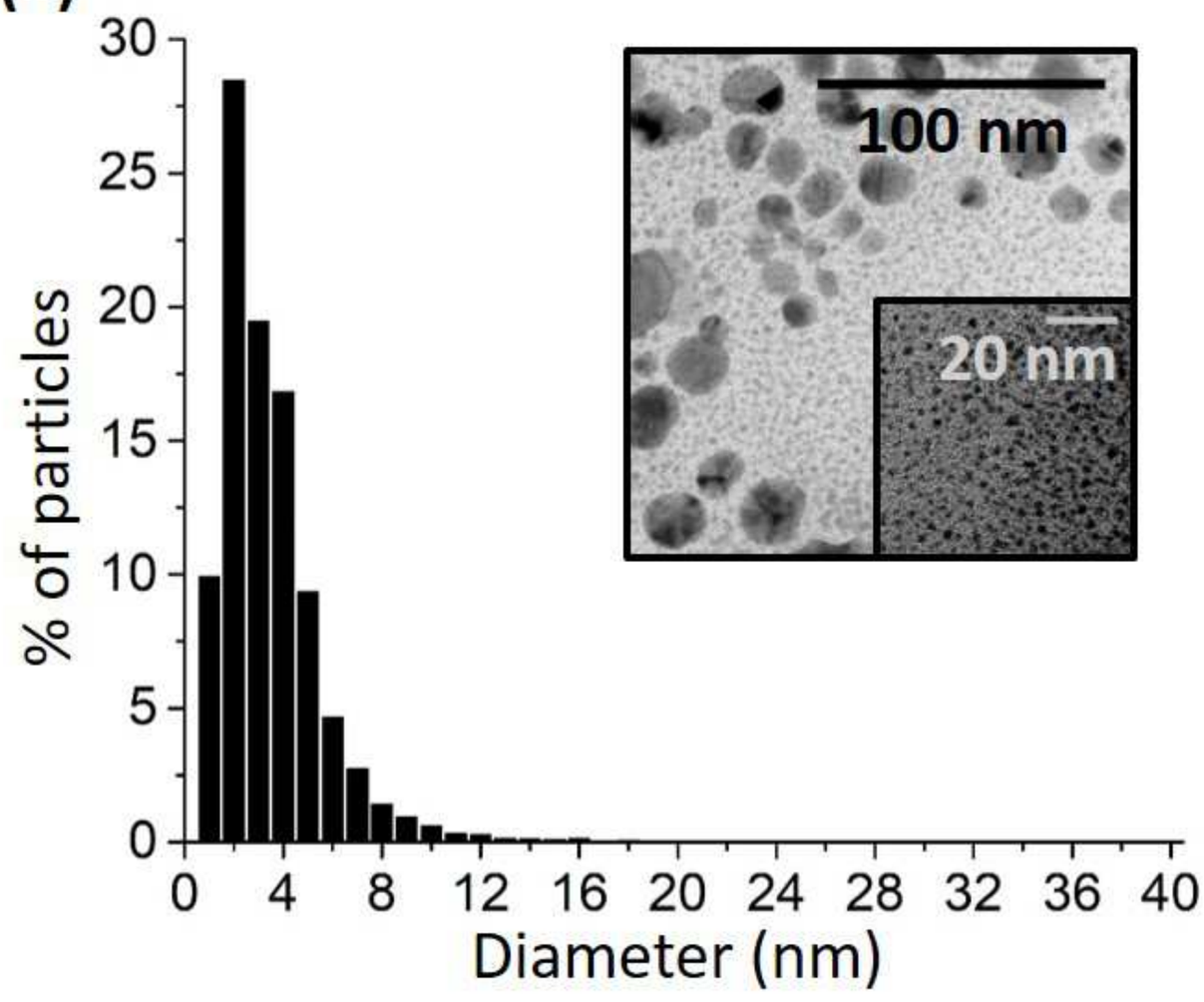
% of particles
Diameter (nm)
100 nm
20 nm

(c)

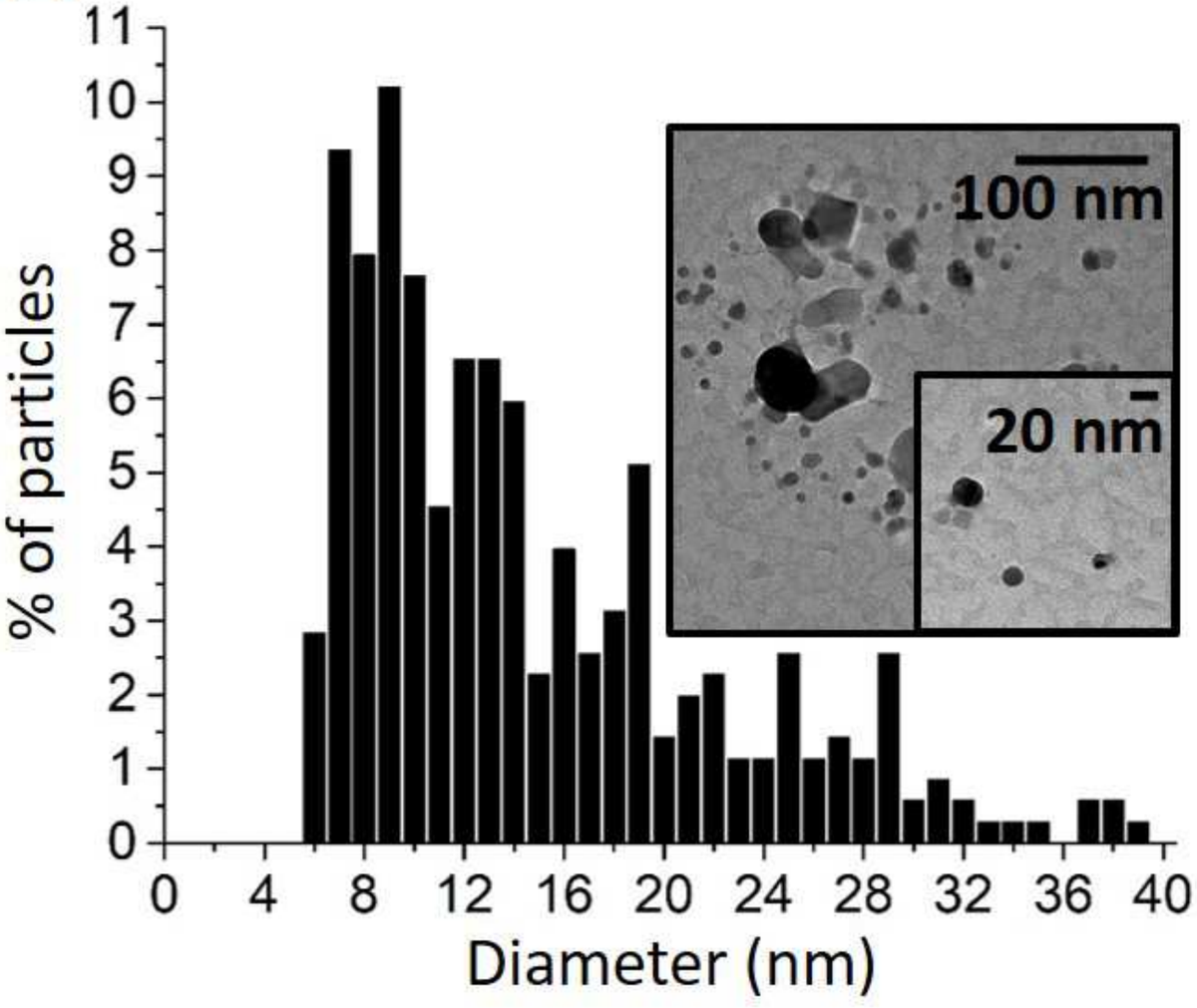
% of particles
Diameter (nm)
100 nm
20 nm

(d)

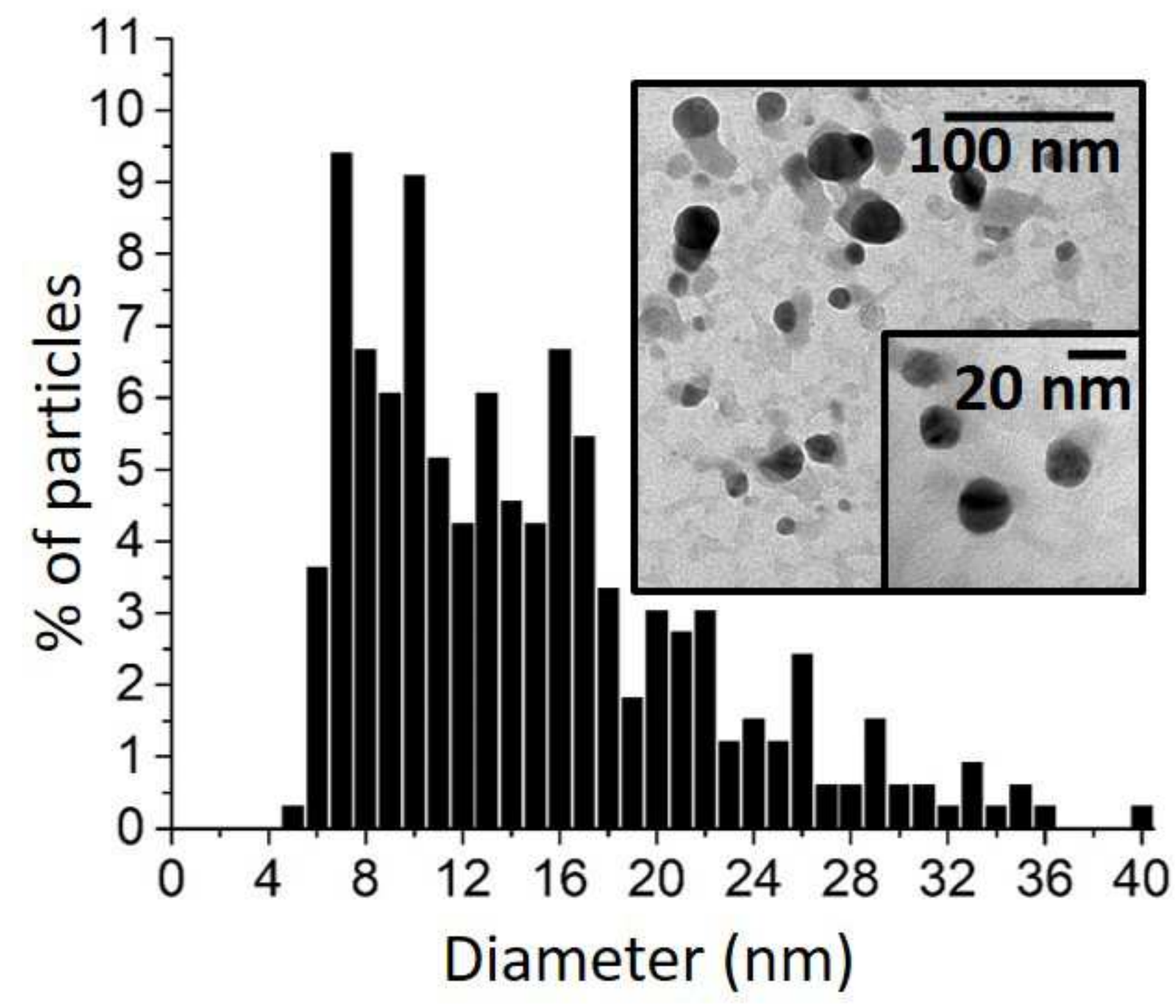
% of particles
Diameter (nm)
100 nm
20 nm

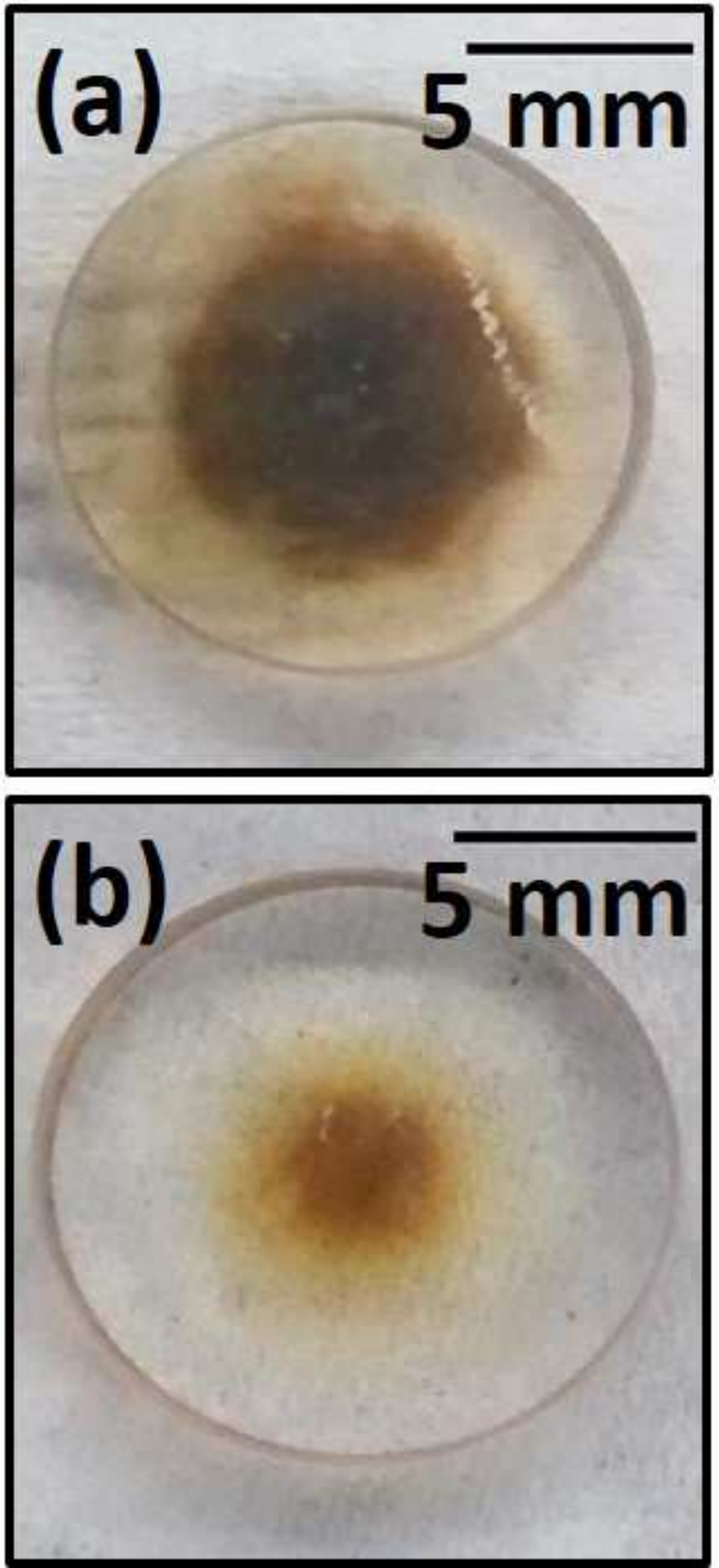
(a)
5 mm
(b)
5 mm
(c)
100 nm
20 nm

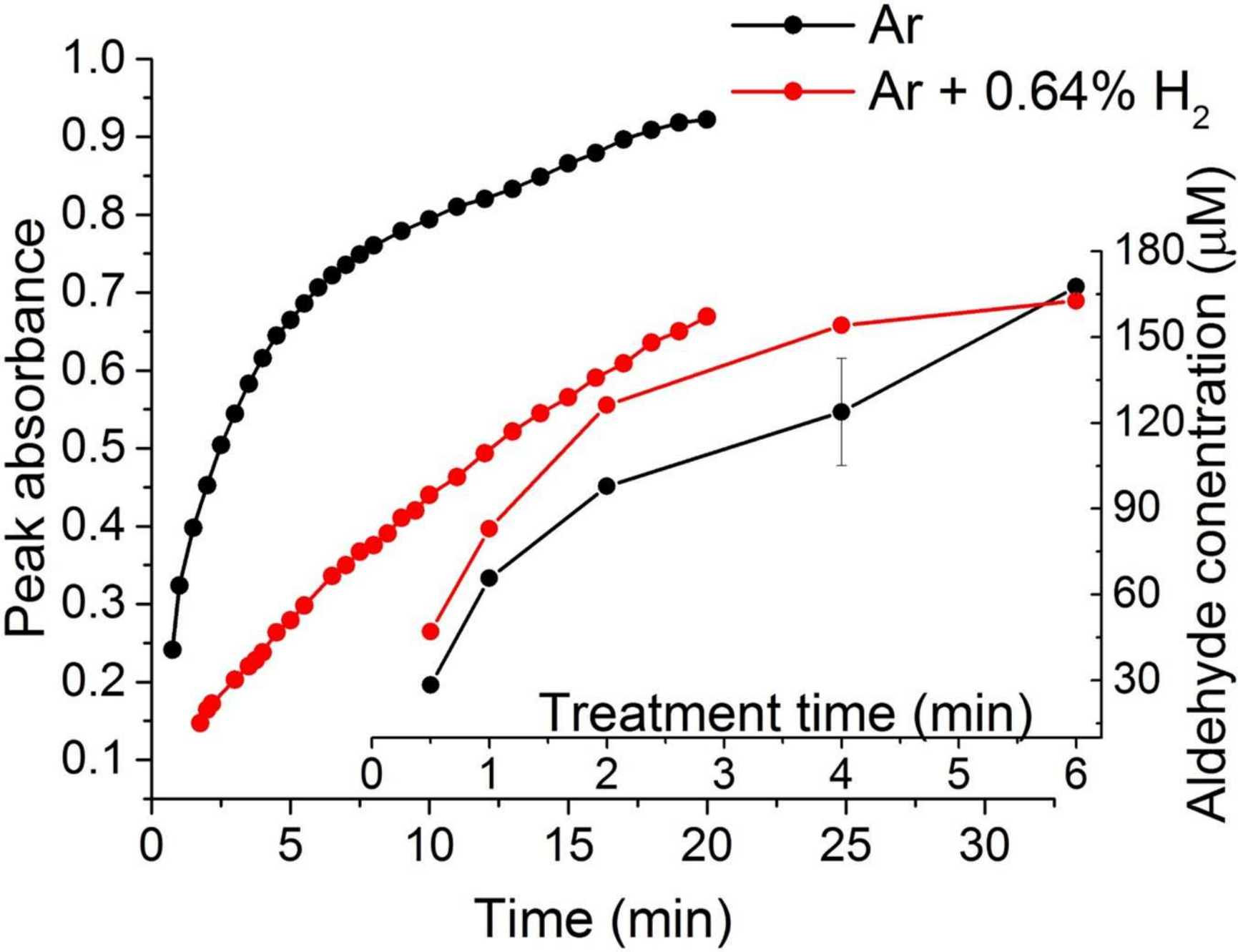
Ar
Ar + 0.64% H2
Peak absorbance
Aldehyde conentration (μM)
Time (min)
Treatment time (min)
1.0
0.9
0.8
0.7
0.6
0.5
0.4
0.3
0.2
0.1
180
150
120
90
60
30
0
5
10
15
20
25
30
0
1
2
3
4
5
6

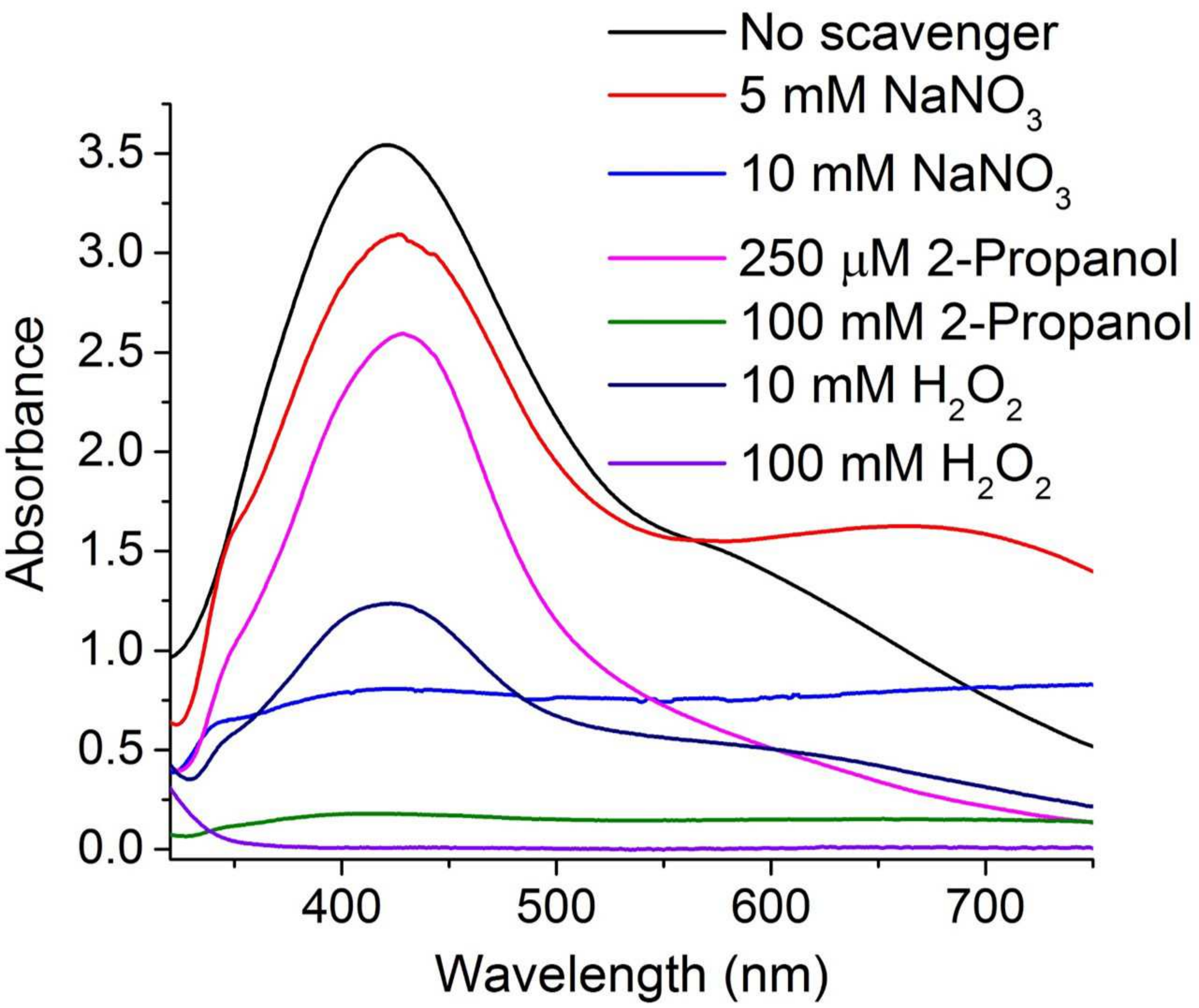
No scavenger
5 mM NaNO3
10 mM NaNO3
250 μM 2-Propanol
100 mM 2-Propanol
10 mM H2O2
100 mM H2O2
Absorbance
3.5
3.0
2.5
2.0
1.5
1.0
0.5
0.0
400
500
600
700
Wavelength (nm)

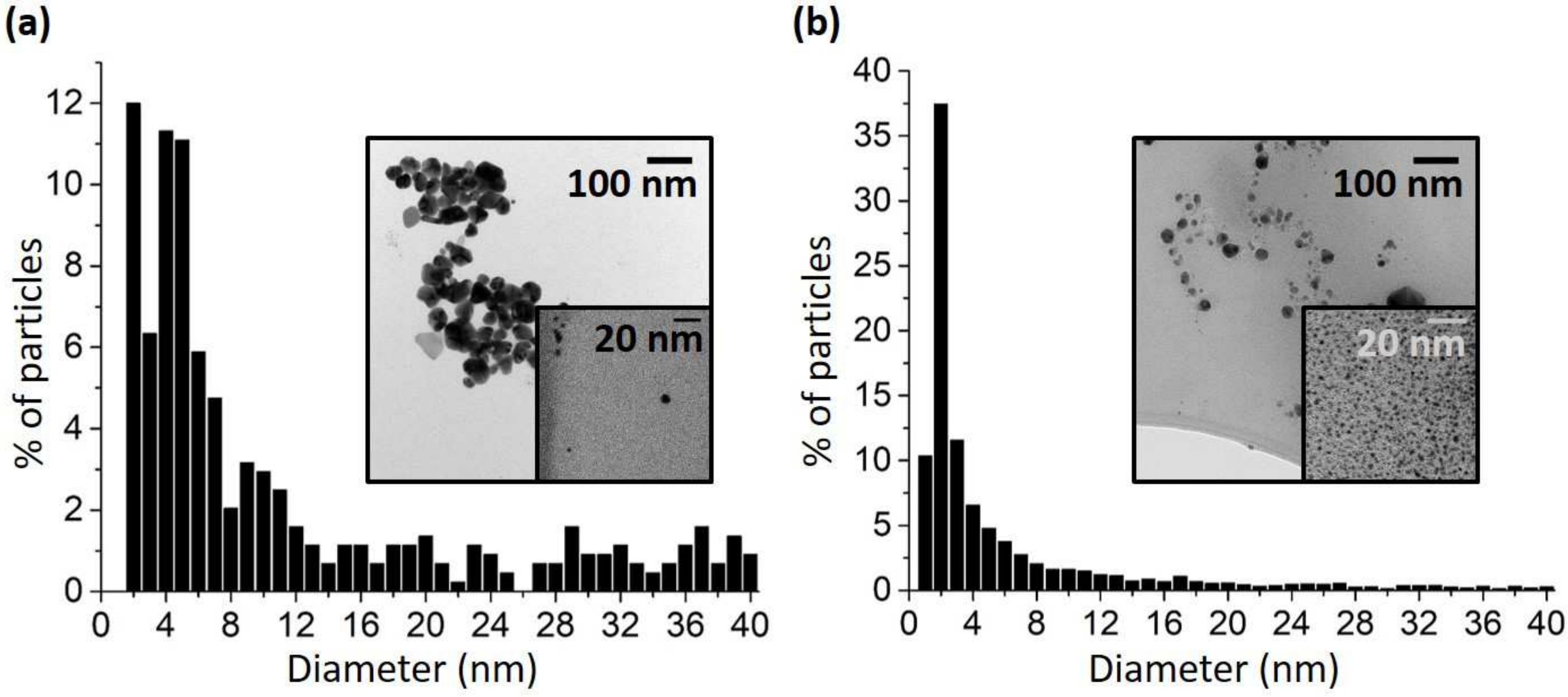
(a)
% of particles
Diameter (nm)
100 nm
20 nm
(b)
% of particles
Diameter (nm)
100 nm
20 nm

(a)

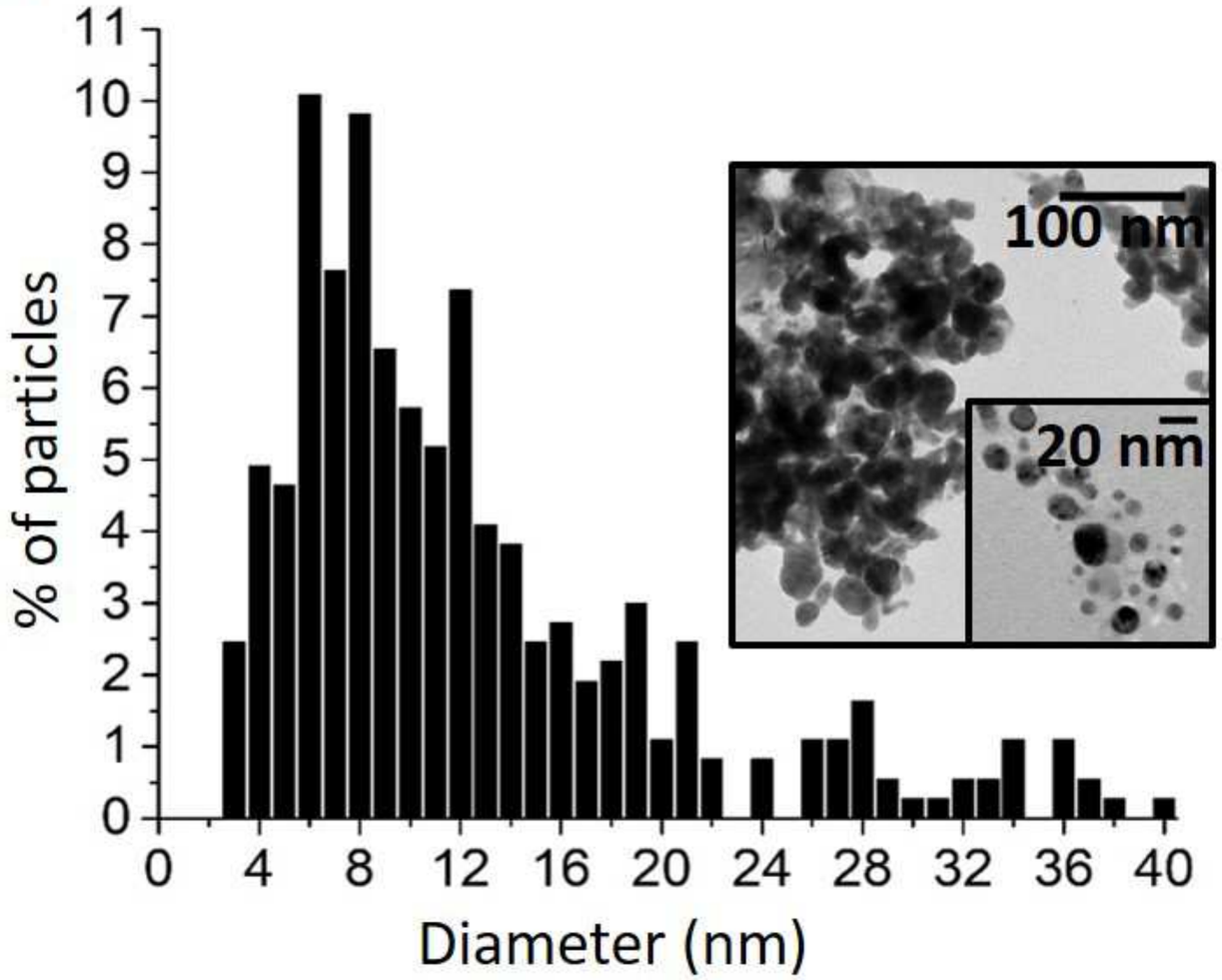
% of particles
Diameter (nm)
100 nm
20 nm

(b)

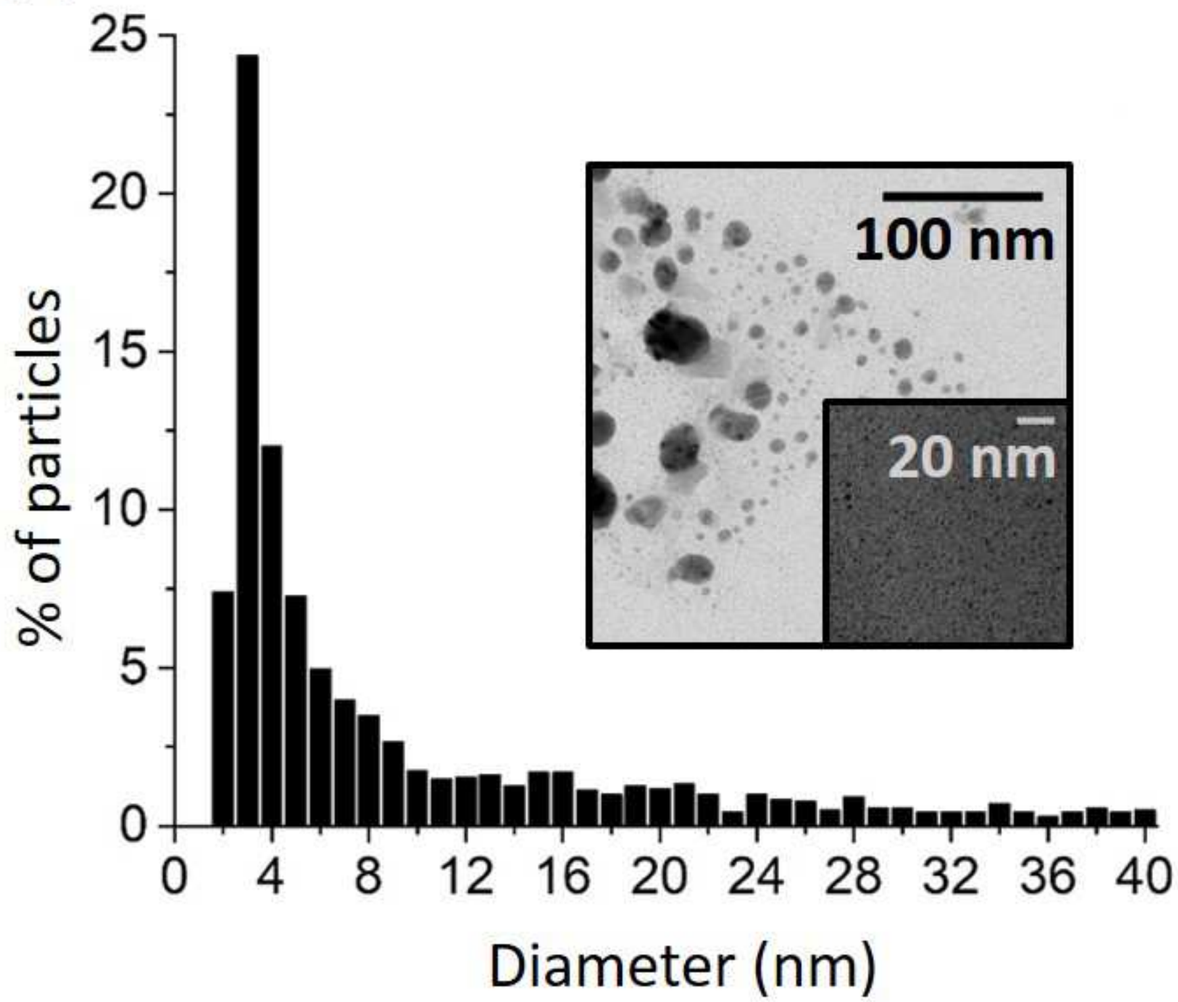
% of particles
Diameter (nm)
100 nm
20 nm

(c)

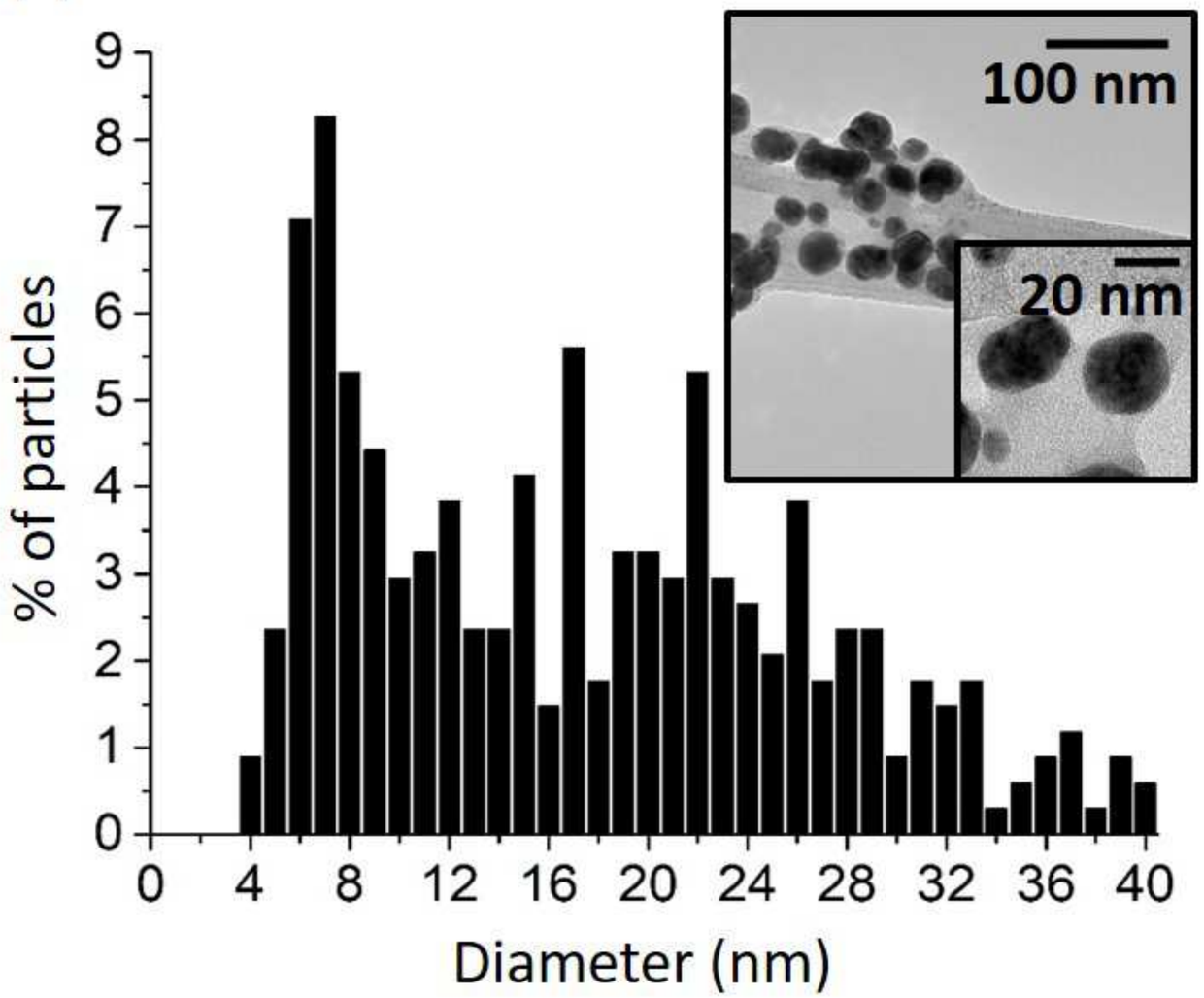
% of particles
Diameter (nm)
100 nm
20 nm

(d)

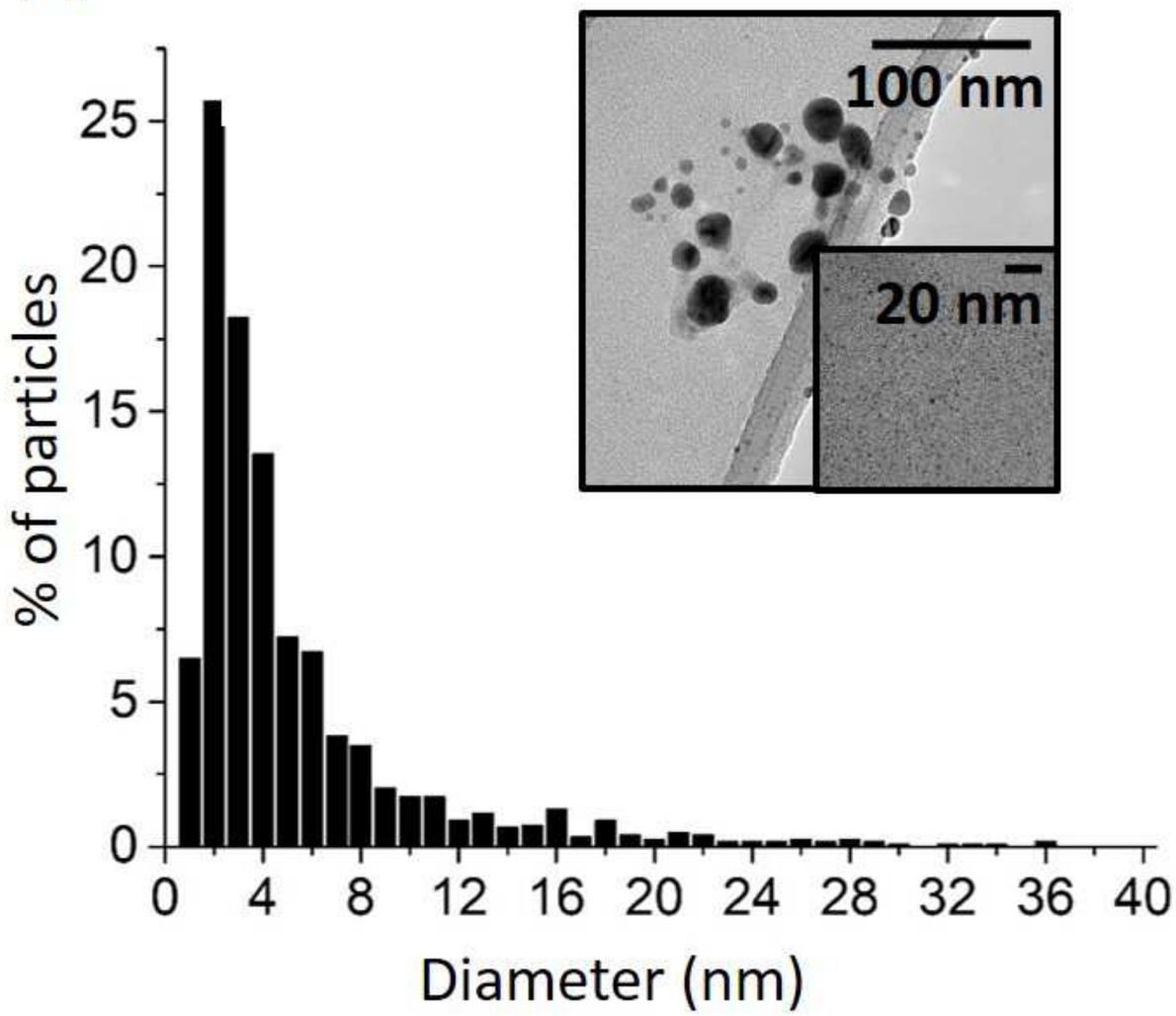
% of particles
Diameter (nm)
100 nm
20 nm

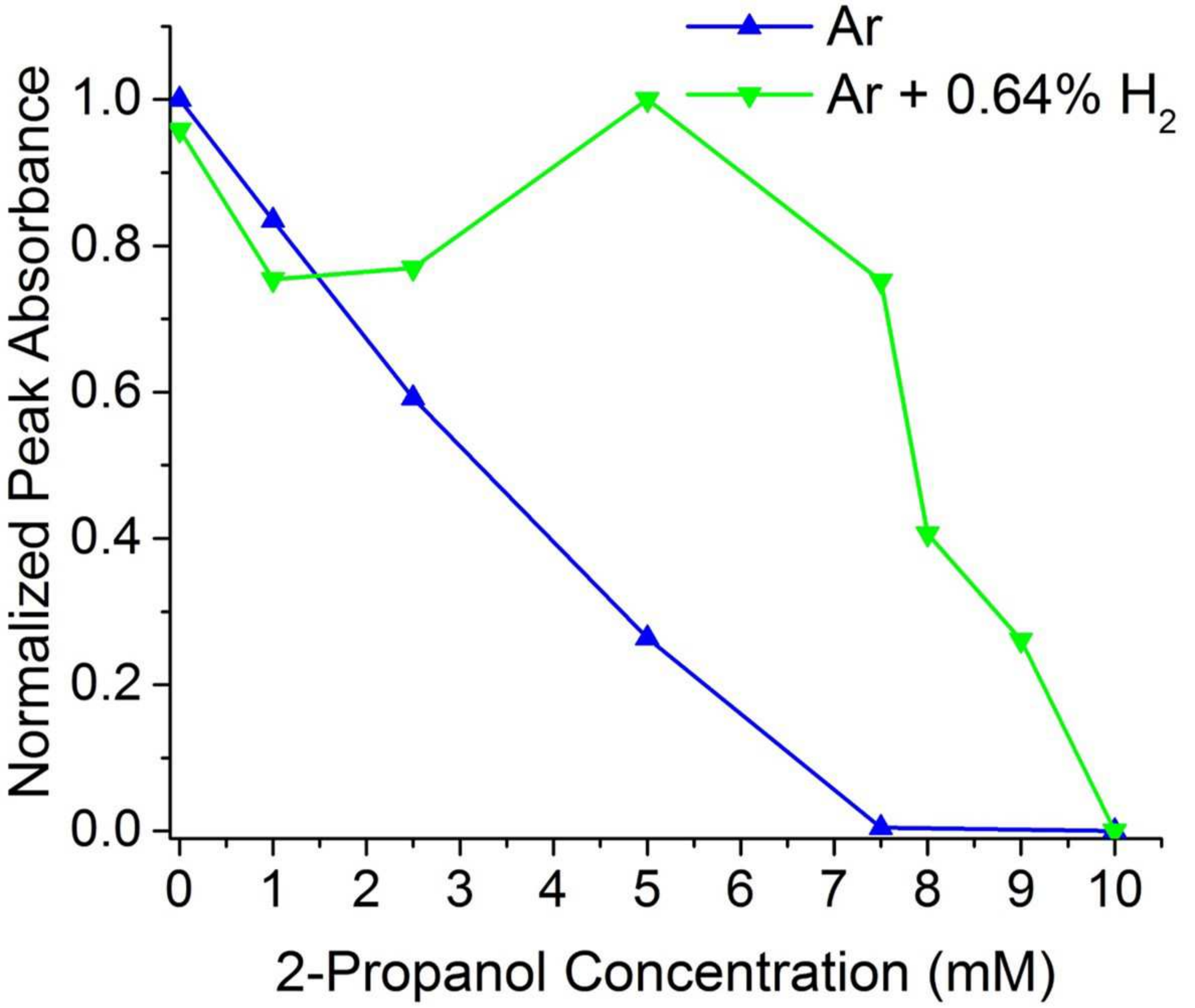
Ar
Ar + 0.64% H2
Normalized Peak Absorbance
1.0
0.8
0.6
0.4
0.2
0.0
0
1
2
3
4
5
6
7
8
9
10
2-Propanol Concentration (mM)